https://doi.org/10.5194/egusphere-2023-2334
Preprint. Discussion started: 6 March 2024

Evaluating the meteorological transport model ensemble for accounting uncertainties in carbon flux estimation over India

Thara Anna Mathew[1,2*], Aparnna Ravi[1,2*], Dhanyalekshmi Pillai[1,2], Lekshmi Saradambal[1,3], Jithin Sukumaran Kumar[1,2], Manoj Manguttathil Gopalakrishnan[4], and Vishnu Thilakan[1,2]

[*]Equally contributing authors
[1]Indian Institute of Science Education and Research Bhopal (IISERB), Bhopal, India.
[2]Max Planck Partner Group at IISERB, Max Planck Society, Munich, Germany.
[3]now at India Meteorological Department (IMD), Pune, India.
[4]Advanced Centre for Atmospheric Radar Research (ACARR), Cochin University of Science and Technology, Kerala, India.

Correspondence: Dhanyalekshmi Pillai (dhanya@iiserb.ac.in)

Abstract. The existing climate change scenario calls for immediate intervention to curb rising greenhouse gas emissions. An improved understanding of the regional distributions of carbon sources and sinks under the perturbed climate system is vital for assisting the above mitigation efforts. The current uncertainties in estimation can potentially be reduced by employing a multi-data modelling system capable of representing atmospheric tracer transport adequately. This study focuses on the mesoscale transport patterns that can affect atmospheric tracer distribution and examines how well they are represented in the meteorological models employed. We investigate the capability of the Weather Research and Forecasting (WRF) model to predict meteorological fields such as temperature, humidity, wind, and planetary boundary layer height (PBLH) by comparing different model simulations with surface and vertical profile observations available at urban and rural stations, Cochin and Gadanki, and with global reanalysis data over India. Combining different model schemes and data products allows us to present a model ensemble of 11 members. Using these ensemble simulations, the impacts of changes in physics schemes, initial and boundary conditions, and spatial resolutions on meteorology and, consequently, on CO_2 mixing ratio simulations are quantified. Most simulations capture variations in temperature and moisture very well (R^2> 0.75). The wind (R^2> 0.75 for height above 2 km) and PBLH simulations (R^2> 0.75 for daytime) are also reasonably correlated with the observations. The sensitivity to changing planetary boundary layer (PBL) schemes and land surface model (LSM) schemes on meteorological and CO_2 mixing ratio simulations is significant, thereby producing higher inter-model differences between experiments. Our analysis provides an assessment of expected CO_2 transport errors when using WRF-like models in the inverse modelling framework. We emphasise the importance of treating these errors in the carbon data assimilation system to utilize the full potential of the measurements and conclude that WRF can be utilised as a potential transport model for the regional carbon flux estimations in India.

https://doi.org/10.5194/egusphere-2023-2334
Preprint. Discussion started: 6 March 2024

1 Introduction

Evidently, anthropogenic perturbations play a major role in causing the current climate crisis by emitting an unprecedented rate of greenhouse gases (GHGs) into the atmosphere. Monitoring GHG emissions, predominantly carbon dioxide (CO_2) and methane (CH_4) and their future projections have thus become paramount for climate change mitigation and adequate policy implementation, focusing on the sustainable development of humankind (Friedlingstein et al., 2020). Combinations of different approaches are required to estimate the anthropogenic and natural sources and sinks of carbon over a region. A multi-data modelling system that combines emission inventories constructed through "bottom-up" approaches, measurements of carbon exchange fluxes, and observations of atmospheric mixing ratios has the potential to improve our understanding of carbon sources and sinks (Bergamaschi et al., 2018; Rödenbeck et al., 2018; Inness et al., 2019). An essential component of the modelling system mentioned above is an atmospheric tracer transport model that predicts the distribution of atmospheric concentrations on a given set of surface fluxes.

The interplay between weather patterns and surface fluxes significantly modulates long-lived greenhouse gases, such as CO_2 and CH_4. The observed variability of these gases is often correlated with the dominant mesoscale weather events in the region (e.g. Van der Molen and Dolman, 2007; Pillai et al., 2016; Parazoo et al., 2008; Lin and Gerbig, 2005; Hedelius et al., 2018; Keppel-Aleks et al., 2011; Agustí-Panareda et al., 2019; Vellalassery et al., 2021; Torres et al., 2019). On a regional scale, tracer transport models employed at coarse resolution often fail to resolve this observed variability (Ahmadov et al., 2009; Gurney et al., 2003). To capture this variability associated with mesoscale events, the tracer transport model needs to advance its Numerical Weather Prediction (NWP) capability and assimilate different meteorological observations. Recent developments in assimilating accurate meteorological information such as air temperature, wind speed, and vertical mixing in the NWP have increased the confidence levels of transport models (Hersbach et al., 2020).

As part of India's emission monitoring and verification in line with the Paris Agreement, we aim to develop a high-resolution modelling framework that provides optimal estimates of CO_2 fluxes by linking atmospheric concentrations to their surface sources and sinks. In this framework, we use a numerical weather prediction model, the Weather Research and Forecasting (WRF). The WRF model is a fully compressible non-hydrostatic model with terrain-following hydrostatic pressure as its vertical coordinate and Arakawa C-grid staggering (Skamarock and Klemp, 2008) which can provide meteorological information to this high-resolution modeling framework.

The present study focuses on the mesoscale transport patterns that affect tracer transport. We investigate the ability of the WRF model to predict the winds and other meteorological parameters as part of a broad goal of deriving Indian CO_2 sources and sinks via inverse modelling. The error in the wind components is one of the significant sources of uncertainty in tracer transport (Hedelius et al., 2018). The biases in simulating temperature variability contribute to the uncertainty in deriving responses of ecosystem respiration and net primary productivity (NPP) (Wang et al., 2013) in cases where biosphere models use modelled meteorological fields. The WRF model has several dynamics, and planetary boundary layer (PBL) modules, and other physical schemes that are suitable for multiple climate conditions. Several studies have investigated the sensitivity of the WRF model to different schemes and parameterizations, with very little agreement regarding which combination gives

https://doi.org/10.5194/egusphere-2023-2334
Preprint. Discussion started: 6 March 2024

the best model performance (Misenis et al., 2006; Li and Pu, 2008; Hu et al., 2010; Sharma et al., 2017; Coniglio et al., 2010; Meyer et al.; Yver et al., 2013). The difference in findings is mostly associated with differences in the study region, surface characteristics, and weather patterns associated with each of them. For example, Feng et al. (2016) showed that the evolution of PBL and associated wind simulations improved greatly for the Los Angeles Basin using a combination of the PBL scheme Mellor-Yamada-Nakanishi-Niino (Nakanishi and Niino, 2004) and a single-layer urban canopy model (SLUCM). Lian et al. (2018) used the WRF model over Paris at 3 km resolution to examine its potential to resolve urban meteorology in comparison with the European Center for Medium-Range Weather Forecast (ECMWF; Hersbach et al. (2020)) data at 16 km resolution. Along with a selection of PBL schemes, they also used Four-Dimensional Data Assimilation (FDDA) in WRF, which approximates the modelled values toward the observations using forcing terms in the equations. A considerable improvement in WRF meteorology has been found with the use of such objective analysis and nudging tools. For the Indian domain, recent studies have used the WRF model and evaluated it against observational and reanalysis data (Gunwani and Mohan, 2017; Bhati and Mohan, 2018; Raju et al., 2015; Mohan and Sati, 2016; Ragi et al., 2020; Kalra et al., 2019; Chawla et al., 2018; Sivan et al., 2021). Most of these studies are either spatially or temporally limited, with a focus on monsoonal patterns and precipitation, or not examining the impact of transport uncertainty on trace gas concentrations.

In this study, we present a detailed analysis for evaluating WRF using available standard near-surface and vertical profiles of meteorological variables (temperature, relative humidity, and wind components) from two geographically unique observation stations over India, Cochin (10.04 °N, 76.33 °E; an urban coastal site) and Gadanki (13.45 °N, 79.2 °E; a rural site). An evaluation using independent reanalysis data is also performed at the regional level. A set of numerical simulations using a combination of different schemes and parameterizations is devised to assess their impact on model biases. The following four main questions are addressed: 1. What are the spatial and temporal error characteristics of the model in capturing the diurnal and monthly variability of temperature, relative humidity, PBL, and winds (both near the surface and upper air) across India? 2. How do the differences in model schemes, parameterizations, and horizontal resolution affect transport errors? 3. What are the sensitivities of the modelled variables to the initial reanalysis fields? 4. How do these transport errors affect the simulation of the CO_2 enhancement?

A description of the observations and the set of simulations generated in this study are presented in Sect. 2. Section 3 provides the quantitative error characteristics of the WRF model when evaluated with observations, including verification with other reanalysis products. An assessment of errors in tracer transport simulations owing to transport model uncertainties is also presented. Section 4 discusses the impact assessments while varying the model schemes, horizontal resolution, and initial reanalysis products. Finally, Sect. 5 provides the conclusions and implications of our results for CO_2 transport.

2 Data and Methodology

2.1 Observations

The vertical profiles of available meteorological variables from radiosonde, Stratosphere-Troposphere (ST), and MicroWave Radiometer (MWR) were used to analyze the efficiency of the model in capturing the observed vertical variations. We also

https://doi.org/10.5194/egusphere-2023-2334
Preprint. Discussion started: 6 March 2024

used surface observations of meteorological variables from an Automatic Weather Station (AWS). Observational data for Cochin were obtained from the Advanced Centre for Atmospheric Radar Research (ACARR). The data used for Gadanki were obtained from the National Atmospheric Research Laboratory (NARL) (website: https://www.narl.gov.in/; last access: 10 March 2023) and are available to the public. Table 1 provides an overview of the geographical features of the study locations and observational data used in this study.

Table 1. Characteristics of the study region. *Discrete observation data.

Station	Cochin	Gadanki
Location (lat, lon)	10.04° N, 76.33° E	13.45° N, 79.2° E
State	Kerala	Andhra Pradesh
Altitude (amsl)	0 m	375 m
Vegetation	Mixed agricultural pattern	Mixed agricultural pattern
Topography	Tropical, Coastal station	Hilly region, Complex terrain
Seasons	Winter (Dec-Jan), Summer/Pre-monsoon (Mar–May), Monsoon (Jun-Sept) and Post-monsoon (Oct-Nov).	Winter (Dec-Jan) Summer/pre-monsoon (Mar–May), Monsoon (Jun-Sept) and Post-monsoon (Oct-Nov).
Urban / Rural	Urban area	Rural area
Instruments used	MWR, Radiosonde, AWS and ST Radar	Radiosonde and AWS
Meteorological variables used	Horizontal wind components, wind speed, wind direction, temperature and moisture.	Horizontal wind components, wind speed, wind direction, temperature and moisture.
Time period of data used	MWR: 09-29 May, AWS: 09-29 May, STR: 26 days* in May, Radiosonde: 13 days* in May 2017.	AWS: 1-31 May, Radiosonde: 25 days* .
Reference	Samson et al. (2016), Mohanakumar et al. (2018), Mathew et al. (2021)	Nath et al. (2010)

2.1.1 ST Radar

The STR at the ACARR, Cochin, operates at 205 MHz with a bandwidth of 5 MHz (Samson et al., 2016). The ∼200 MHz band radar has a height coverage from 0.315 km to 20 km and beyond. This study used mode-1 of the STR (45 m vertical resolution, 0.315 km to 8 km altitude) measurements. The STR measures horizontal and vertical wind components continuously at 9-minute intervals, and data are available for approximately 26 days in May 2017. The data are mostly continuous from the forenoon to evening hours and throughout the day for some days (Samson et al., 2016). Kottayil et al. (2016) validated STR data with collocated radiosonde observations for 1 to 6 km and reported the ability of STR to provide good quality atmospheric wind measurements for the given range.

https://doi.org/10.5194/egusphere-2023-2334
Preprint. Discussion started: 6 March 2024

Table 2. Summary of physics schemes and parameterizations of the numerical experiments used in the study.

Set 1		PBL + SL
Expt 1	Microphysics – WSM3, Longwave radiation – RRTM,	MYNN3 + MYNN
Expt 2	Shortwave radiation – Dudhia, LSM – Unified Noah LSM,	YSU + Revised MM5
Expt 3	Cumulus parameterization – Grell Freitas (GF)	MYJ + Eta Similarity
Expt 4		ACM2 + Revised MM5
Set 2		LSM
Expt 5	Microphysics – WSM3, Longwave radiation – RRTM,	RUC
Expt 6	Shortwave radiation – Dudhia,	Noah – MP, PBL – MYNN3,
Expt 7	Cumulus parameterization – Grell Freitas (GF)	SL – MYNN, CLM4
Set 3		LSM+Urban Model
Expt 8	Microphysics – WSM3, Longwave radiation – RRTM,	Unified Noah+UCM
Expt 9	Shortwave radiation – Dudhia,	Noah-MP+UCM
	Cumulus parameterization – Grell Freitas (GF),	
	PBL – MYNN3, SL – MYNN.	
Set 4		Nested run
Expt 6	Microphysics – WSM3, Longwave radiation – RRTM,	Single domain, 10 km × 10 km
Expt 10	LSM – Noah – MP,	Outer domain, 9 km × 9 km,
	Shortwave radiation – Dudhia,	Inner domain, 3 km × 3 km
	Cumulus parameterization – Grell Freitas (GF),	
	PBL – MYNN3, SL – MYNN	
Set 5		Initial condition
Expt 6	Microphysics – WSM3, Longwave radiation – RRTM,	ERA-5
Expt 11	Shortwave radiation - Dudhia, SL - MYNN	NCEP FNL (Final) operational
	Cumulus parameterization – Grell Freitas (GF),	global analysis and forecast data.
	LSM - Noah – MP, PBL – MYNN3	

2.1.2 GPS Radiosonde

The Global Positioning System (GPS) sonde (GRAW, DFM-09), used for upper air studies at ACARR, Cochin measures the altitude, pressure, temperature, relative humidity, wind speed, wind direction, and geographical position (latitude/longitude). The sonde measurements are made using an ultra-modern and resistant ceramic temperature sensor, humidity sensor, and the

https://doi.org/10.5194/egusphere-2023-2334
Preprint. Discussion started: 6 March 2024

integrated GPS module that determines the position, wind direction, and wind speed. The flights were around 14:00 LT and gave continuous observation every five seconds until the balloon burst. Intermittent data for 13 days in May 2017 were used in this study (Mohanakumar et al., 2018). We also used observations from a high-resolution GPS radiosonde (RD-11G, Meisei) provided by the NARL at Gadanki (Nath et al., 2010). A majority of these radiosondes were launched during afternoon hours (approximately 17.30 LT) and provided vertical profiles of temperature, pressure, relative humidity, wind speed, wind direction, and geographical position up to the balloon-burst altitude (approximately 30 to 35 km). The present study utilized all available radiosonde vertical profiles (25 days) at 16.30 and 17.30 LT in May 2017 from Gadanki.

2.1.3 Microwave Radiometer

We used MWR profiler data obtained as part of a monsoon onset campaign (MONset, 2017), jointly organized by ACARR and the Indian Institute of Tropical Meteorology (IITM), Pune (Mathew et al., 2021). The Radiometer model MP-3000A was used for the campaign. The instrument provides vertical profiles of temperature and moisture continuously every couple of minutes with a 50 m resolution for 0 to 1 km height, 100 m for 1 to 2 km, and 250 m for 2 to 10 km. The data were continuously available from 10 to 29 May 2017.

2.1.4 AWS

The AWS at ACARR, Cochin uses a Campbell Scientific data logger (Campbell Scientific, Inc.), with a data logger (CR3000) and sensors for air temperature and relative humidity (Vaisala HMP45), wind speed and direction (RM Young 05103), air pressure (RM Young 61302 V), and a net radiometer (Kipp & Zonen, model CNR4-B) (Manoj et al., 2021). The AWS provides surface-level data of meteorological parameters such as air temperature, relative humidity, wind speed, surface pressure, and net solar radiation, with a temporal resolution of one minute. The data from 9 to 29 May 2017 were used for this study.

The AWS setup at Gadanki under the Indian Space Research Organization (ISRO) initiative provides surface meteorological parameters. The wind speed, wind direction, air temperature, air humidity, and atmospheric pressure (Reddy et al., 2015) at the surface were recorded every second and provided as hourly mean data. The hourly mean data of these surface parameters from 1 to 31 May 2017 for Gadanki were also used to analyze the model performance in simulating observed surface features.

2.2 Model set-up

2.2.1 General configuration

In this study, version 3.9.1.1 of Advanced Research WRF (ARW; Skamarock and Klemp (2008)) was used to generate the simulations for 2017 from May 01, 00 UTC to May 31, 18 UTC. A set of 11 model experiments (Table 2) were designed for the current study, in which the model re-initialization was set to 30 h, and a model spin-up time of the initial 6 h was allowed. The fifth-generation ECMWF reanalysis data ERA5 (Hersbach et al., 2020) with hourly intervals, 31 km grid resolution, and a vertical resolution of 91 levels up to a height of 21 km were used to provide the initial and boundary conditions for the model ensemble members (simulation experiments) from 1 to 10 (hereafter referred to Expt. with corresponding numbers).

https://doi.org/10.5194/egusphere-2023-2334
Preprint. Discussion started: 6 March 2024

For Expt. 11, the National Centers for Environmental Prediction (NCEP FNL (Final)) operational global analysis and forecast data on 0.25°× 0.25° grids and 32 vertical levels prepared operationally every six hours (https://doi.org/10.5065/D65Q4T4Z; last access: 10 March 2023) was used as initial and boundary conditions. All models were run with a spatial resolution of ∼10 km, enclosing the entire Indian subcontinent, as shown in Fig. 1 for all ensemble members except Expt. 10. In Expt. 10, an outer domain covering the same region but with a resolution of ∼9 km × 9 km was embedded with a two-way nested domain of horizontal resolution ∼3 km × 3 km that included the study sites of Cochin and Gadanki (inner domain). All models were run with a vertical resolution of 39 levels from the surface and reached up to a height of ∼20 km with 8 levels within 1.5 km from the surface. Static land-use data with a temporal resolution of 30 s provided by MODIS were also used. The time integration in the model uses the third-order Runge–Kutta scheme and the spatial discretization uses second-to sixth-order schemes.

2.2.2 Numerical experiments

In this study, we analysed the sensitivity of model forecasts towards different physical schemes and parameterizations used, primarily the PBL schemes (Set 1), Land Surface Models (LSM) (Set 2), and Urban Model (UM) (Set 3) (See Table 2). In addition, we examined the impact of horizontal resolution (Set 4) and different initial and boundary conditions (Set 5) on the meteorological variables (See Table 2). The PBL scheme parameterizes the unresolved turbulent vertical fluxes of heat, momentum, and moisture within the planetary boundary layer and throughout the atmosphere. Some PBL schemes are tied to particular Surface Layer (SL) schemes available in the WRF model, so a fixed surface layer scheme cannot be used (Skamarock and Klemp, 2008). Thus, we used four different pairs of PBL and SL schemes for the first set of simulation experiments, whereas all other physics schemes were fixed. The microphysics scheme used was the WSM3 (WRF Single-Moment Class 3) scheme, which is suitable for mesoscale grid processes (Hong et al., 2004), and the cumulus parameterization used was the Grell-Freitas scheme (GF) (Grell and Freitas, 2014). The radiation physics schemes used were Dudhia (Dudhia, 1989) and RRTM (Mlawer et al., 1997) for shortwave and longwave radiation, respectively. The Unified Noah LSM (Mukul Tewari et al., 2004) was coupled with the WRF for parameterization of land surface processes, and no urban models were coupled with WRF for these sets of experiments. The PBL schemes used were the Mellor-Yamada-Nakanishi-Niino Level 3 (MYNN3) scheme (Nakanishi and Niino, 2006, 2009), Yonsei University (YSU) Scheme (Hong et al., 2004), Mellor-Yamada-Janjic (MYJ) scheme (Janjić, 1990, 1994), and Asymmetrical Convective Model version 2 (ACM2) scheme (Pleim, 2007). The surface fluxes required for the PBL scheme are provided by the surface layer and land surface schemes. By convention, while the Revised MM5 surface layer (Jiménez et al., 2012) scheme is tied to the YSU and ACM2 PBL schemes, the Eta Similarity scheme (Janjić, 1990, 1994; Janić, 2001) with the MYJ PBL scheme, and the MYNN scheme is used along with the MYNN3 PBL scheme.

Land surface processes strongly affect weather and climate from local to regional and global scales by controlling the surface energy balance and water balance (Zhao and Li, 2015). LSM provides heat and moisture fluxes over land to provide a lower boundary condition for vertical transport in the PBL scheme. These sensible heat and latent energy fluxes depend on surface meteorology, radiative forcing, soil properties, and land use type. Thus, an accurate description of the land surface and

https://doi.org/10.5194/egusphere-2023-2334
Preprint. Discussion started: 6 March 2024

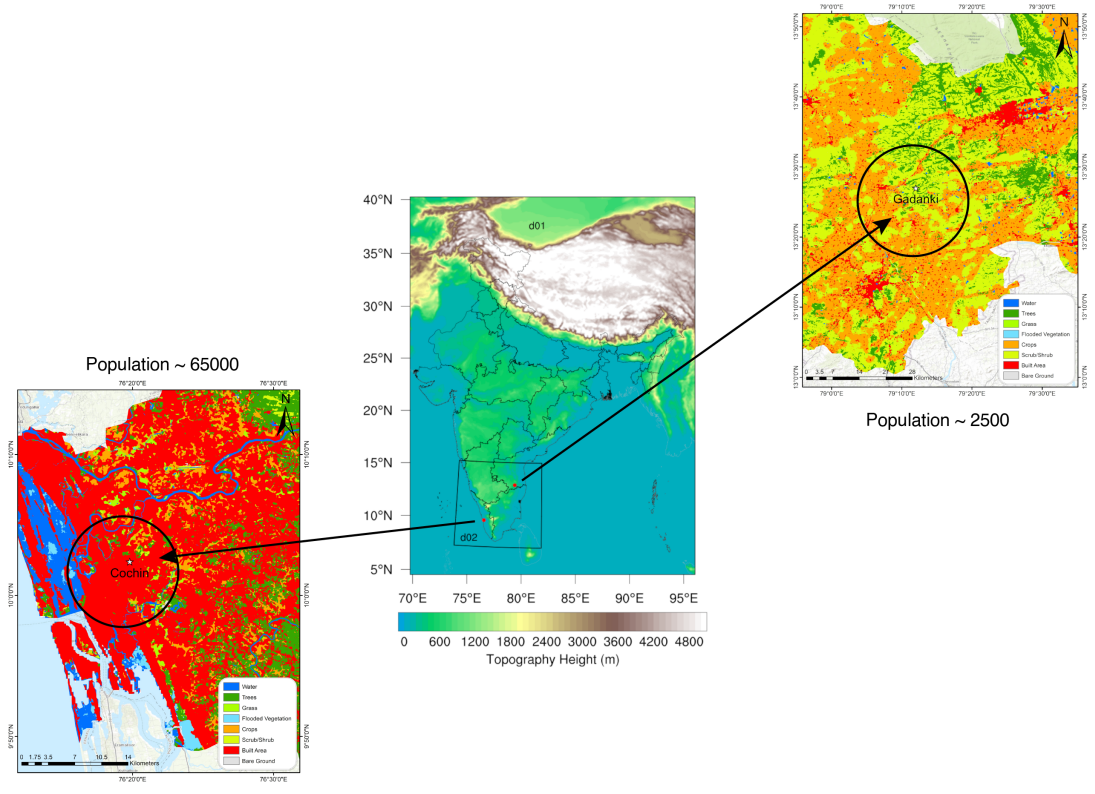

Figure 1. Map of model domains and the location of observational sites used in the study overlaid on topographical height. The parent domain covers the entire region shown, and the inner domain covers the polygon shown inside the parent domain. The left and right figures show the land use land cover map using ESRI global LULC 10m map (2020) surrounding the observational sites.

vegetation characteristics is needed in any numerical weather prediction model for better performance (Wharton et al., 2013).
170 The second set of experiments was designed by fixing them onto a single PBL and SL pair and changing the LSMs. Here, we fixed the PBL-SL scheme pair in Expt. 1, and the land surface models used included (Expt(s). 5 to 7) RUC (Benjamin et al., 2004), Noah-MP (multi-physics) (Niu et al., 2011; Yang et al., 2011), and Community Land Surface Model (CLM4; Lawrence et al. (2011); Jin and Wen (2012); Lu and Kueppers (2012); Subin et al. (2011); Oleson et al. (2010)), in addition to the Unified Noah LSM used earlier in Expt. 1.

175 Land Use Land Cover (LULC) change, urban geometry, and anthropogenic heat emissions in urban areas affect the surface energy budget by creating heat islands, generally inducing lower winds and modifying wind direction (Lee et al., 2011; Bonacquisti et al., 2006). In Set 3 of the experiments, we coupled the Urban Canopy Model (UCM; Kusaka et al. (2001); Kusaka and Kimura (2004); Chen et al. (2004)) to both Noah LSMs, that is, Unified Noah (Expt. 1), and Noah multiphysics (Expt. 6). Thus Expt. 8 and 9 are the same as Expt. 1 and 6, respectively, are coupled with an urban model (UCM). Accounting for urban

https://doi.org/10.5194/egusphere-2023-2334
Preprint. Discussion started: 6 March 2024

effects in high-resolution meteorological fields may improve emission estimates by better modelling CO_2 concentrations over large urban areas (Feng et al., 2016; Nehrkorn et al., 2013).

Using a fixed set of physics schemes as in Expt. 6, we conducted two additional WRF runs (Expt. 10 & 11), each considering a different aspect other than the physical parameterizations and schemes, which are the impacts caused by a higher horizontal resolution and a different set of initial conditions. In this set, WRF was run (a) with a nested domain covering the study sites of Cochin and Gadanki (Expt. 10). The inner domain has two-way nesting with a horizontal resolution of 3 km, and the parent domain covers the same region as earlier, with a resolution of 9 km and (b) the same as Expt. 6, but with a different set of initial and boundary conditions provided by the NCEP FNL (Final) operational global analysis and forecast data (Expt. 11). A summary of the numerical experiments is provided in Table 2.

2.3 Gridded data and reanalysis products

Daily gridded maximum and minimum temperature data at 1° × 1° spatial resolution provided by the Indian Meteorological Department (IMD) were used to evaluate the spatial temperature representation by the models. This dataset uses quality-controlled temperature data from hundreds of stations across India, which are interpolated into grids using a modified version of Shepard's angular distance weighting algorithm (Shepard, 1968). Daily maximum and minimum temperature data for May 2017 that are limited to the Indian domain were used in this study. Further information can be found in Srivastava et al. (2009).

We used the ERA-Interim reanalysis dataset (Berrisford et al., 2011), namely 'Surface or single level' data for May 2017 that includes 2D parameters such as temperature at 2m, wind speed, and wind direction at 10 m. The dataset has a spatial resolution of 0.125°×0.125° and a temporal resolution of 3 h (Uppala et al., 2008; Dee et al., 2011). Such a comparison with the model experiments allows us to examine how the physics schemes of the regional model modify the initial data with time and what differences arise with the change in version.

Additionally, we used the Modern-Era Retrospective analysis for Research and Applications version 2 (MERRA-2) (Gelaro et al., 2017) reanalysis data generated by the Goddard Earth Observing System Model, Version 5 (GEOS-5) with its Atmospheric Data Assimilation System (ADAS), version 5.12.4. We used assimilated meteorological fields for temperature and wind, with a temporal resolution of 3 h and with a spatial resolution of 0.5°×0.625° (https://gmao.gsfc.nasa.gov/; last access: 10 March 2023).

2.4 Estimation of observation-based PBL height

We derived the Planetary Boundary Layer Height (PBLH) from available MWR data for 10 to 30 May 2017. The Holzworth (Holzworth, 1964) and Stull (Stull, 1988) methods were used for the calculation. In the Holzworth method, the PBLH is derived based on the potential temperature, where the surface parcel is lifted dry-adiabatically until it intersects the sounding profile. If a surface inversion exists, the PBLH is derived based on the top of the inversion. Otherwise, it is identified as the base of a lifted inversion (within 4 km of the above-ground level). The Stull method is similar to the Holzworth method, except for the use of the virtual potential temperature parcel instead of the potential temperature. The virtual temperature was calculated from the MWR data. The above two methods have resulted in two PBLH datasets derived from the observations, hereafter referred

https://doi.org/10.5194/egusphere-2023-2334
Preprint. Discussion started: 6 March 2024

to as PBLH (Holzworth) and PBLH (Stull). We also used the mean PBLH (referred to as PBLH (avg)) calculated from these two datasets to evaluate simulated PBLH.

2.5 Data pre-processing for model evaluation

Table 1 provides an overview of the observation datasets used in this study. For surface data analysis, we derived the diurnal averages of the observations and simulations. The data from the MWR (See Sect. 2.1.3) were aggregated into a monthly timescale representing 10 different time steps to evaluate the models during the day (10:30, 12:30, 14:30, 16:30, and 18:30 LT) and night (22:30, 0:30, 2:30, 4:30, and 6:30 LT). A similar daytime classification was applied to the STR data (See Sect. 2.1.1). We averaged the radiosonde data at 14:30 LT (average radiosonde flight time) from Cochin to obtain the variations at the monthly scale. For Gandanki, the radiosonde data between 16:30 LT and 17:30 LT were used to calculate the monthly mean. (See Sect. 2.1.2). The vertical profile data analysis considered observed variables from the surface to a height of 8 km. Bin-wise averages of 0-1, 1-2, 2-3, ... up to 7-8 km have been performed here. Model simulations from the grids nearest to the observational sites were used for this model-data comparison. All WRF experiments were interpolated to the nearest observational vertical level to evaluate the vertical variation in meteorological variables. Continuous ground observations from AWS were considered for the surface data analysis for both sites. The simulations and the corresponding observations were aggregated into hourly, diurnal, and monthly time scales for the analysis done throughout the study. We also examined the coefficient of determination (R^2), Root Mean Square Error (RMSE), and Mean Bias Error (MBE) between WRF ensemble simulations and observations at a monthly scale.

To compare gridded and reanalysis data products, hourly WRF simulations were regridded to match the spatial and temporal resolutions of corresponding data products.

2.6 Simulation of CO_2 mixing ratio

By coupling the meteorological fields derived from the 11 model simulations with the Stochastic Time Inverted Lagrangian Transport (STILT) Model v2.3 (Lin et al., 2003; Gerbig et al., 2003; Nehrkorn et al., 2010), we made an ensemble simulation of CO_2 mixing ratio enhancements. We performed backwards STILT trajectories that are driven by 11 WRF-model ensemble members, derived the influence matrix (as a measure of the sensitivity of mixing ratios to the upstream fluxes) (Gerbig et al., 2003; Thilakan et al., 2023; Pillai et al., 2013; Kariyathan et al., 2020), and mapped them with anthropogenic fluxes to make ensemble simulation of CO_2 mixing ratio enhancements over Cochin and Gadanki. The time-invariant annual emission flux from the Emission Database for Global Atmospheric Research (EDGAR) (EDGAR v7.0; Crippa et al. (2020, 2021)) at a spatial resolution of $0.1° \times 0.1°$ was used. We utilized these simulations to assess the CO_2 variability caused by the differences in meteorological fields. The uncertainty associated with the CO_2 mixing ratio simulations (11 ensemble members) was calculated as the standard deviation of differences normalized by their mean. The quantification of variations in CO_2 mixing ratio simulations due to different model realizations is explained by the spread among each set of experiments. Set 4 is not considered here since the WRF nested domain is much smaller than the STILT domain. To quantify the individual influence

https://doi.org/10.5194/egusphere-2023-2334
Preprint. Discussion started: 6 March 2024

of variability in PBL height, wind speed, and temperature simulated by different WRF experiments on the CO_2 mixing ratio enhancement simulations, simple linear regression analysis is also performed.

3 Results

3.1 Meteorological evaluation and error characteristics

3.1.1 Surface variables

The monthly averaged diurnal variations in surface temperature, relative humidity (RH), wind speed, and wind direction from the observational sites are shown in Fig. 2. The model simulations agree with observations in capturing the diurnal variability in temperature for both sites (R^2> 0.95 for Cochin and R^2> 0.75 for Gadanki). Despite the high degree of correlation between observation and model simulations, there exists a slight negative bias (underestimation) in the modelled surface temperature at Cochin, irrespective of the different schemes and parameterizations used (See Fig. S1). A spread in the range of 1 °C to 3 °C (based on RMSE) from the observed mean is found in all models for these sites. A time lead of ∼2 h is seen in surface temperature simulations compared to observations over Gadanki, and Madala et al. (2014) also reported similar modelling limitations. While a cold bias (∼-2 °C to -4 °C) is found during nighttime (18:30 to 4:30 LT), the daytime (5:30 to 17:30 LT) simulations exhibit a warm bias (∼1 °C to 2 °C) over Gadanki (See Fig. S1), similar to previous studies (Kadaverugu et al., 2021; Boadh et al., 2016; Hariprasad et al., 2014; Mohan and Bhati, 2011). Daytime (RMSE= 2.1 °C, MBE = -3.5 °C) predictions at Gadanki are slightly closer to the observations than night-time (RMSE= 2.5 °C, MBE = -2.5 °C) predictions with high R^2 (=0.9). On the other hand, Cochin simulations of temperature are better during nighttime (daytime: RMSE= 1.8 °C, MBE = -1.7 °C; nighttime: RMSE= 0.8 °C, MBE = -0.8 °C).

The monthly mean RH at sites follows strong diurnal variability (Figs. 2c and 2d). All model experiments captured the observed diurnal variation in RH over both locations with good correlation (R^2> 0.9 for Cochin and > 0.8 for Gadanki) but overestimated the values (MBE of 12% to 20% for Cochin and 3% to 19% for Gadanki). Higher RH values of ∼ 70-85% are generally observed during nighttime, compared to daytime values (∼30-60% depending on the sites). Similar to the surface temperature, the diurnal pattern in RH at Gadanki also showed a lead of 1 to 2 h, except for Expt. 7 (See Fig. S2) and reported a good correlation (R^2> 0.9) with observations (Fig. 2d), but with a large bias. In contrast, the Expt. 7 poorly simulated diurnal variations of RH for Cochin (R^2= 0.4). The inter-model spread for RH (0.04%) is slightly greater during noon and afternoon hours than during the rest of the time, as in the case of surface temperature (0.01%), but with a larger spread than that of temperature. Using different LSMs (Set 2) causes a larger variance than when PBL (Set 1) and UCMs (Set 3) are changed in simulating surface temperature and relative humidity. The intermodal differences for RH are greater during the daytime for all sets of experiments.

The observed diurnal variations in wind speed at Gadanki are fairly captured by the models (R^2> 0.5) (Fig. 2e). All models overestimate the diurnal variability in wind speed. Changes in PBL, LSMs, and UCMs in the WRF experimental design do not seem to improve the model's ability to capture the observed diurnal patterns in wind speed. Inter-modal differences are found

https://doi.org/10.5194/egusphere-2023-2334
Preprint. Discussion started: 6 March 2024

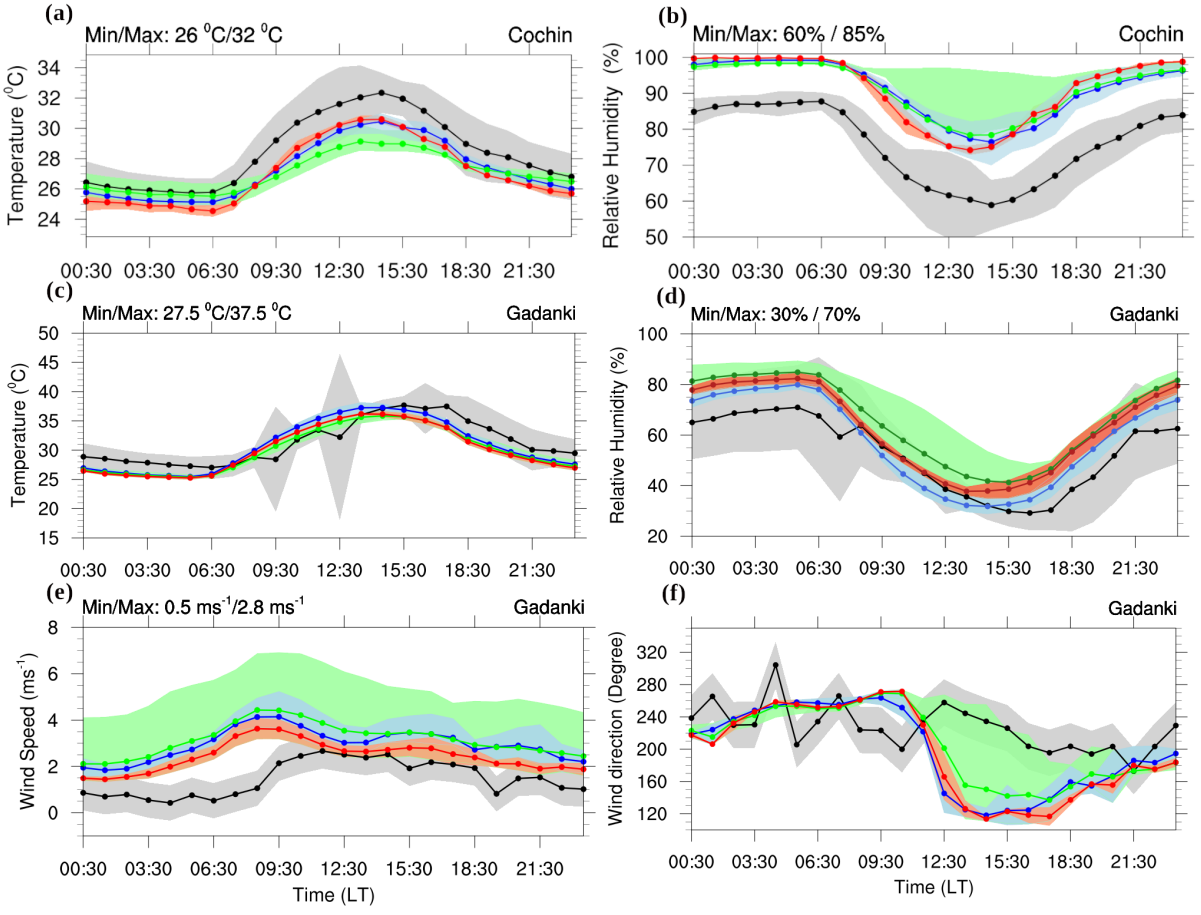

Figure 2. Mean and standard deviation in the monthly averaged diurnal variation of Temperature at 2 m and Relative Humidity at 2 m for Cochin (a & b) and Gadanki (c & d). e & f represent the wind speed and direction at 10 m, respectively, at Gadanki. Grey shade (solid line) shows +/- 1 standard deviation (mean) of observation, and blue, green, and salmon shades (solid lines) show the range of +/- 1 standard deviation (mean) obtained from Set 1, 2, and 3 experiments, respectively.

to be greater when different LSMs are applied. A large inter-model spread is found in daytime, similar to previous studies (Hariprasad et al., 2014; Kadaverugu et al., 2021; Madala et al., 2013, 2015; Sathyanadh et al., 2017). Figure 2f indicates a poor correlation between the simulated and observed wind directions, with a RMSE range of 30° to 65°. Experiment 7 shows a slight improvement in reproducing the observed monthly diurnal pattern in wind direction (Fig. S2). Surface winds over Gadanki during May 2017 were predominantly south westerlies (Fig. 2f). However, most of the models simulate south easterlies during afternoon hours (12:30 LT to 16:30 LT), showing difficulties in capturing random fluctuations in the wind direction.

https://doi.org/10.5194/egusphere-2023-2334
Preprint. Discussion started: 6 March 2024

3.1.2 Vertical Profiles

Here, we compare the vertical profiles of meteorological variables with simulations. Using MWR observations, the set-wise model performance (See Table 2) of temperature variability with height (for bins of equal height levels, 0-1,1-2,..7-8 km) was analyzed. The vertical profile of mean and standard deviation of bias (model - observation) in temperature (daytime (10:30 LT) and nighttime (22:30 LT); See Fig.3) shows underestimation (peak of ∼-2 °C in the lower levels (< 2 km) and overestimation (∼3 °C) towards higher levels (> 3 km). The nighttime profile shows an underestimation below 2 km as well. However, in both cases, the 5 sets of experiments align more in the higher levels (> 3 km). Figure 4 considers four different periods of a day to account for the overall diurnal evolution of the boundary layer. The periods 07:30 to 15:30 LT (excluding 15:30 LT), 15:30 to 19:30 LT (excluding 19:30 LT), 19:30 to 01:30 LT (excluding 01:30 LT), and 01:30 to 07:30 LT (excluding 07:30 LT; hereafter referred to as t1, t2, t3, and t4), all in local time, are considered here as the representative periods for an unstable, unstable-to-stable, stable and stable-to-unstable boundary layer conditions respectively. A strong variation exists in the model-observation correlation with height, and the correlation varies drastically among models irrespective of time. Comparatively low R^2(< 0.5) values are seen for t3 and t4 (where stable conditions prevail). In general, simulated temperature profiles show an underestimation in the lower levels and an overestimation in the middle to upper levels with MWR observations, showing no considerable inter-model variability in the upper levels (Fig. S3). In addition, a higher daytime bias is seen when the boundary layer is unstable (08:30 LT to 17:30 LT).

Further, a comparison with the vertical profiles is made using the available radiosonde observations (13 days) at 14:30 LT for May 2017 (See Sect. 2.5). The monthly averaged simulated temperature profiles agree with the observations at both sites. Apart from the high correlation, a significant model-observation bias exists for temperature, which decreases at higher altitudes (> 4 km). All models underestimate the vertical variations in temperature at Cochin, with maximum underestimation in the ground level (mean bias of ∼ -1.7 °C to 0.7 °C), but overestimation is found at Gadanki above ∼4.5 km. The highest correlation (R^2> 0.99) is found in the middle to the upper atmosphere, together with a low RMSE and bias (< 0.5 °C). Figure 5 shows the set-wise vertical profile of mean and standard deviation in the bias of temperature, RH, wind speed and wind direction, respectively, over Cochin (Fig. 5a-d) and Gadanki (Fig.5 e-g). The vertical axis shows bins of altitude 0-1,1-2,..7-8 km, corresponding to which the mean and standard deviation of bias have been analysed. Considerable influence of different PBL, LSM, and UCMs in simulating the vertical temperature profile is noticed over both stations (See Figs. 5a & e). The monthly averaged radiosonde vertical profiles of RH are well represented (R^2> 0.85) by the models at both locations but with a slight overestimation in the lower levels (0 to 2 km). Overall, we find that RH is sensitive to changes in the PBL, LSMs and UCMs (indicated as Set 1-3). In the lower levels (up to 1.5 km), there is an overestimation of 5 to 13 % (according to the mean bias in Fig. 5b considering Set 1-5) while it decreases to a range of -3 to -6 % at ∼ 3 km showing underestimation of RH. Models overestimate RH in the upper levels (0 to 6 % at ∼ 7 km). Evidently, the experiments are closer to each other in the higher levels than the lower levels. The standard deviation in bias is also higher in the bins 0-2 km. Also, the low levels at Gadanki show overestimation. However, in contrast to Cochin, the vertical profile mean bias in RH shows a clear pattern of overestimation until ∼ 5 km and further underestimation (Fig. 5f). The standard deviation in bias is slightly higher above 4 km compared to the lower altitudes.

https://doi.org/10.5194/egusphere-2023-2334
Preprint. Discussion started: 6 March 2024

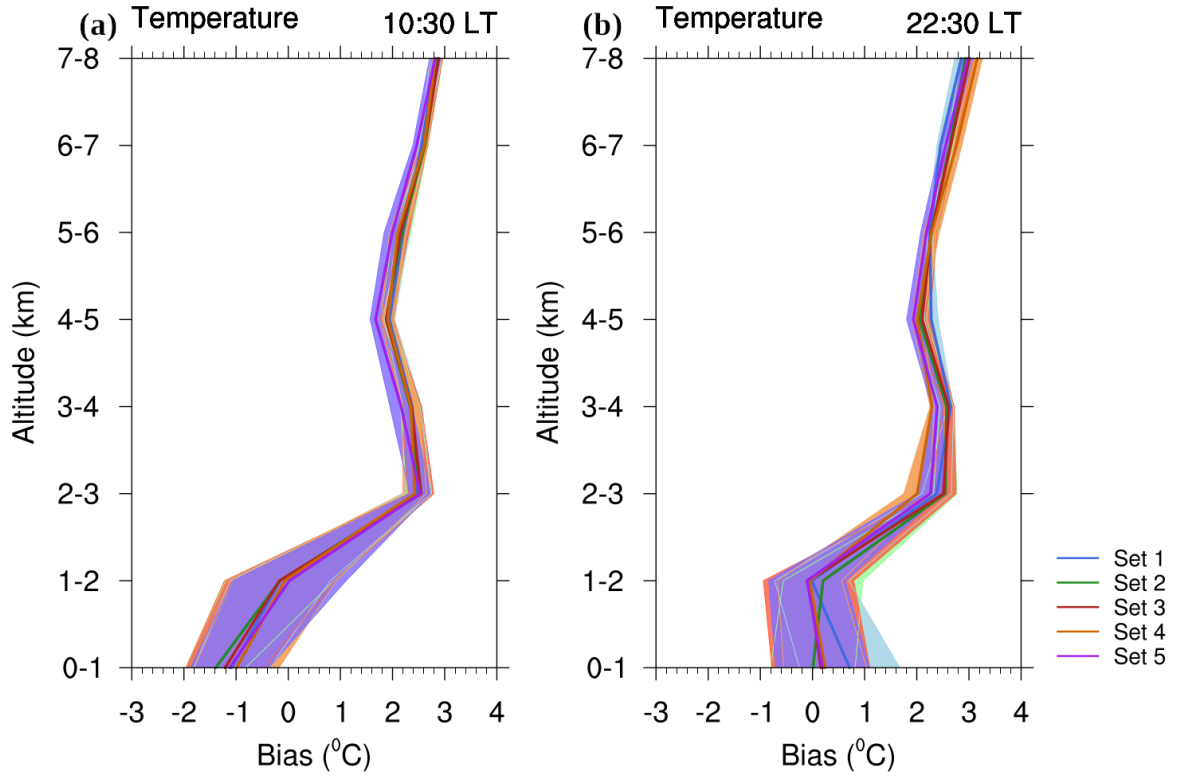

Figure 3. Mean and standard deviation in the bias of monthly averaged vertical profile of temperature by each set of experiments at Cochin averaged over every 1 km interval from 0 to 8 km at 2 different time steps in a) daytime (10:30 LT) and b) nighttime (22:30 LT) against observational MWR profile. Solid vertical lines show the mean bias, and shades show the +1/-1 standard deviation of bias from the mean for each set of experiments.

Wind simulations are better above 2 km, while the pattern is poorly captured within 0 to 2 km level. The least mean bias in wind speed is seen at ∼4 km over Cochin and at ∼3 km over Gadanki.

Besides radiosonde observations, hourly vertical profiles of wind from the STR were analyzed over Cochin (Fig. S4). Even though the models capture the wind speed, the model-data mismatch is considerable in the morning. Large inter-model differences in wind speed occur at the boundary layer, which decreases with altitude. Meanwhile, an increase in the intermodel spread in wind speed is found in the afternoon. The correlation coefficients are greater for the higher altitude (> 2 km) profiles. All model simulations generally underestimate wind speed. This contrasts with the behaviour of the modelled wind speed at 10 m (See Sect. 3.1.1). It is noteworthy that Expt. 7 (MYNN+CLM4 combination) captures the vertical wind speed profile remarkably well with high R^2 values. The underestimation of wind speed and the inadequate representation of mixing can contribute to uncertainties in trace gas transport and its quantification. The diurnal variation in the bias between the monthly mean wind speed from the STR observations and WRF experiments shows a large negative bias, except for the CLM4 scheme,

https://doi.org/10.5194/egusphere-2023-2334
Preprint. Discussion started: 6 March 2024

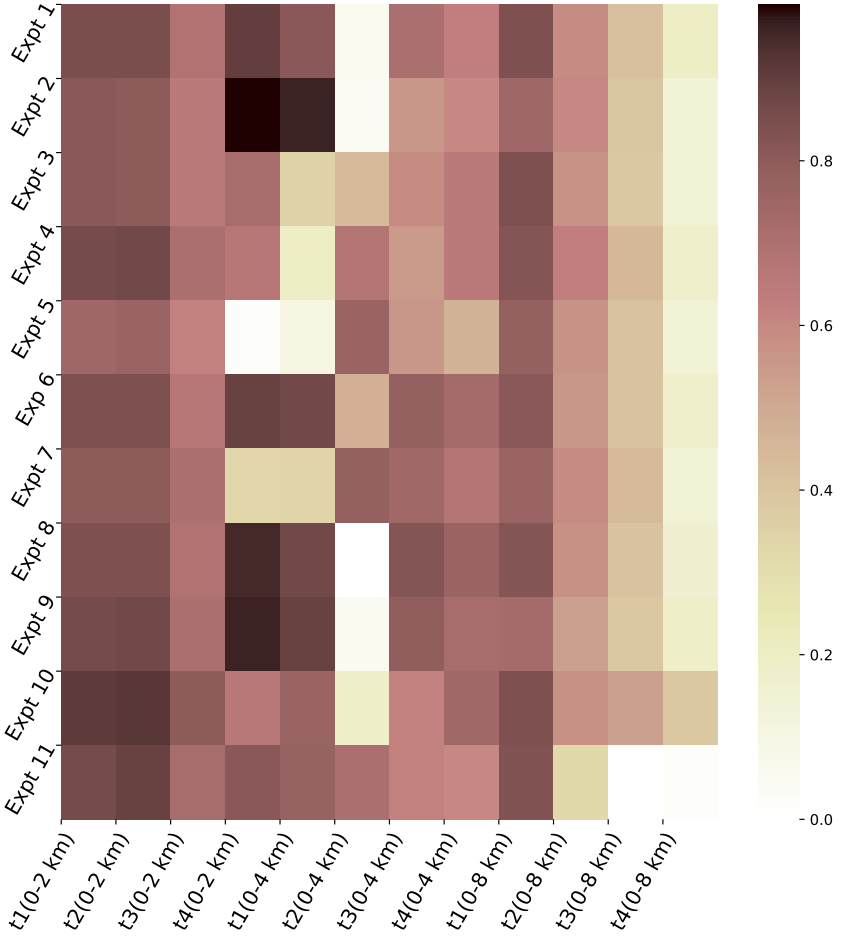

Figure 4. Vertical profiles in the correlation (R^2; for time slabs t1 to t4) of monthly averaged temperature at Cochin for 0 to 8 km height during four different time periods of a day for all the numerical experiments with respect to observational MWR data.

which simulates near-zero biases. The wind bias is minimal within the 2 to 4 km level, while a large negative bias in the lower levels and a large positive bias in the higher levels are evident. Wind-direction profiles are also derived from the horizontal wind components of the STR. Like the wind speed, the R^2 values are better in higher altitudes. The inter-model differences are the highest at the boundary layer and increased in the afternoon. Overall, Expt.7 (MYNN+CLM4) and Expt.5 (MYNN+RUC) combinations perform better with high R^2 values. Figure 6 shows the mean bias and its standard deviation for vertical wind profiles for morning (10:30 LT) and evening (16:30 LT) from observational STR profiles. Similar to the findings above, Fig. 6 indicates a large mean bias in the lower altitudes (< 2 km) in comparison with higher altitudes (> 2 km). The wind bias is

https://doi.org/10.5194/egusphere-2023-2334
Preprint. Discussion started: 6 March 2024

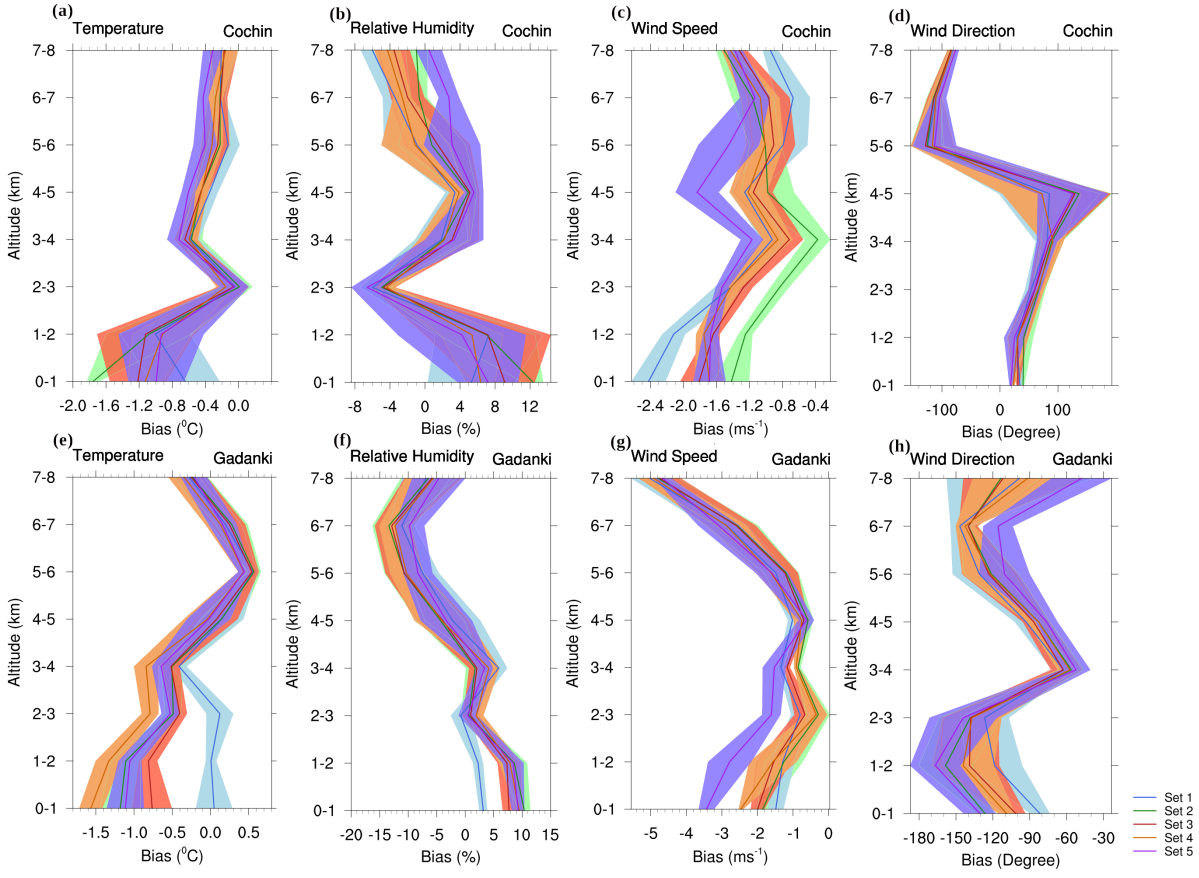

Figure 5. Mean and standard deviation in the bias among WRF simulated monthly averaged vertical profiles of a) temperature, b) relative humidity, c) windspeed, and d) wind-direction against radiosonde observations at Cochin around 14:30 LT and at Gadanki (e-h) for May 2017 averaged over 16:30 and 17:30 LT.

larger in the evening hours in comparison with that of the morning. Figure 7 shows the diurnal variation in the bias between the monthly mean wind speed from the STR observations and WRF experiments. The wind speed near the ground shows a large negative bias, except for the CLM4 scheme, which simulates near-zero biases. The bias is minimum within the 2 to 4 km level, while a large negative bias in the lower levels (0 to 2 km) and a large positive bias in the higher levels (4 to 8 km) were evident.

3.2 Evaluation of PBLH

PBLH simulations are compared with the observationally derived PBLH (See Sect. 2.4) for Cochin. PBLH estimated using the Stull method shows maximum PBL height during 12:30 to 13:30 LT, while the Holzworth method indicates maximum PBLH during 14:30 LT (Fig. 8a). The model simulations are closer to the Stull method in capturing the diurnal pattern with a lead time of ∼3 h. However, the simulated estimation is closer to the Holzworth method for capturing the timing of the peak

https://doi.org/10.5194/egusphere-2023-2334
Preprint. Discussion started: 6 March 2024

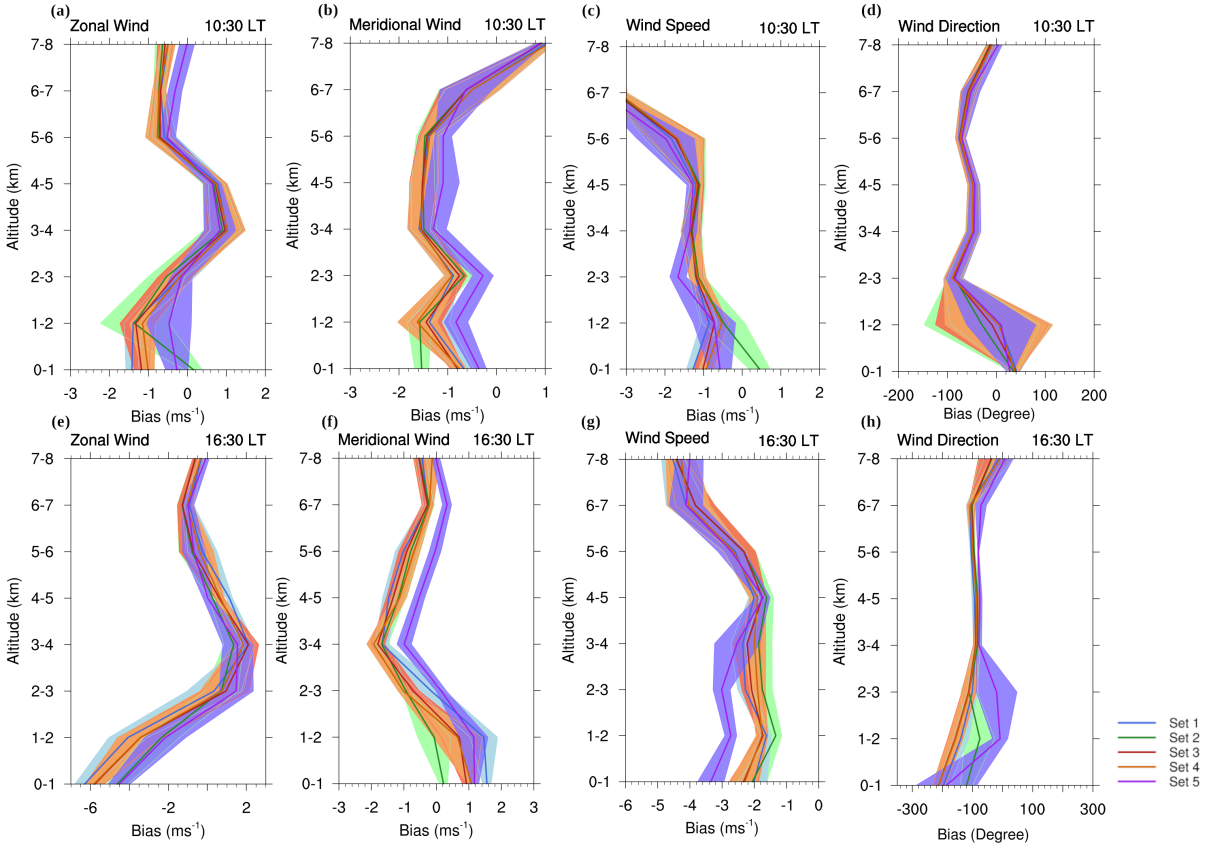

Figure 6. Mean and standard deviation in the bias among WRF simulated monthly averaged vertical profiles of a) & e) zonal wind, b) & f) meridional wind, c) & g) wind speed, d) & h) wind direction against observational STR profile from 0 to 8 km at Cochin at 2 different time steps of the day (10:30 LT and 16:30 LT).

PBLH. The diurnal profile analysis shows that the monthly averaged stable boundary layer simulations in Expt. 1, 2, and 3 are farther from the observation (Fig. 8a). Models' difficulties in simulating stable boundary layers and dynamics have already been widely discussed in previous studies (Guo et al., 2021; Seidel et al., 2012; de Arruda Moreira et al., 2018). A large spread exists among the PBLH estimation methods used, and the sensitivity of PBLH to changes in LSM schemes is greater than that of PBL and UCM schemes, as seen in Fig. 8b.

Table 3 provides the statistics for various sub-sample periods (7:30 to 15:30 LT, 15:30 to 19:30 LT, 19:30 to 1:30 LT, and 1:30 to 7:30 LT), assessing the model performance in the diurnal conditions of convective stability. The models generally agree with observational-based PBLH (R^2> 0.6). Most model experiments underestimate PBLH, especially for unstable hours (See Table 3). The RMSE values are found to be higher for unstable periods than that for stable periods. The above results align with the previous study, comparing PBL heights in reanalysis datasets and radiosonde observations (Guo et al., 2021). A significant underestimation of the PBL height in reanalysis datasets against radiosonde observations was reported by them. The large

https://doi.org/10.5194/egusphere-2023-2334
Preprint. Discussion started: 6 March 2024

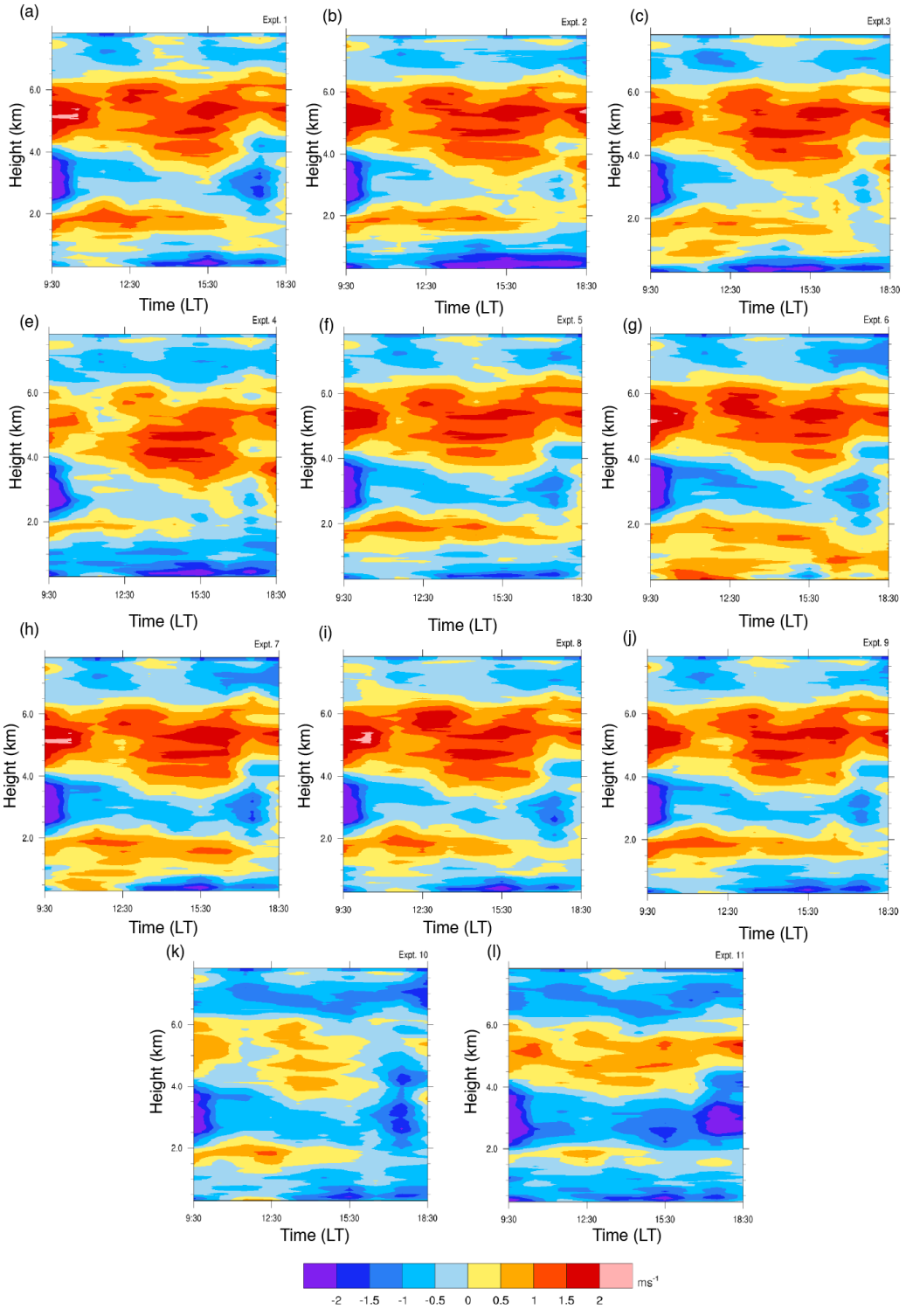

Figure 7. Diurnal variation of the monthly averaged bias in wind speed among STR observations and WRF simulations over Cochin for May 2017 for Expt. 1 to 11.

https://doi.org/10.5194/egusphere-2023-2334
Preprint. Discussion started: 6 March 2024

underestimation of the PBLH can potentially induce uncertainties in boundary-layer trace gas distributions, as discussed in Sect. 4.

3.3 Comparison with gridded and reanalysis data products

Here, we examine the general agreement of our model simulations with other observational and model-based datasets. Our model simulations largely agree with IMD's maximum and minimum temperatures (R^2< 0.64). However, we find significant temperature differences over the Himalayan region when comparing all model simulations and IMD data (See Fig. 9).

Using ERA-Interim and MERRA-2 reanalysis products, we compared monthly mean spatial patterns of WRF models' meteorological variables for daytime (5:30 to 17:30 LT) and nighttime (18:30 to 4:30 LT; Figure not shown). Daytime comparison of WRF temperature at 2 m with ERA-Interim shows good spatial agreement with less bias (between -1 °C and 1 °C) and high correlation (R^2> 0.81) (Fig. S3). However, the correlation with ERA-Interim is noticeably weak over southwestern India (R^2 ∼-0.01). A narrow band of negative bias (∼-8 °C) over the Himalayan ranges and positive bias over the rest of the subcontinent are persistent in the nine WRF-ERA simulations (Expt 1-9). All simulations show positive differences over Central India and Southern India, except for Expt. 6 (Figure not shown), with a negative difference of ∼-5 °C over the region. Expt. 2, 3, and 4 show the highest positive bias over the Indian land mass and surrounding oceanic regions. The region shows a negative difference during the night, with the northern region showing a higher difference than the rest. The correlation between our models and ERA-Interim is higher during the day than at night. Overall, good agreement (R^2> 0.64) in the spatial pattern of wind variables between the WRF experiments and ERA-Interim is found. The analysis shows considerable differences in coastal regions, indicating differences in simulating coastal fine-scale dynamics. Our simulations are closer (higher correlation) to ERA-Interim during the daytime than during the night. The PBLH simulations by WRF are in good agreement (R^2> 0.64) with the Era-Interim throughout the domain, except for the coastal and northernmost mountainous regions, where the correlation is very weak (R^2< 0.25) (Figure not shown). The correlation is higher during the daytime than at night. Expt. 1 to 3 are closer to the reanalysis product than Expt. 4 to 11.

In the case of comparison with the MERRA-2 reanalysis product, the surface temperature comparisons show a good correlation (R^2> 0.64) over the Indian region (Figure not shown). The daytime temperature is highly correlated with reanalysis data than the nocturnal temperatures. A strong negative correlation in western oceanic regions is found in Expt. 2, 3, and 4. The Southern and northeastern parts of the country show a minimum correlation with the MERRA-2 surface temperature. The spatial difference in PBLH is mostly∼-500 m. The bias values become increasingly less negative over the coastal regions. Also, daytime values show a larger negative bias than nighttime values, indicating the magnitude of PBL height model simulations is considerably lower than the reanalysis during the day. A similar case of large negative bias in the unstable hours has been identified by comparing with observation data over Cochin, as well (See Section 3.2).

3.4 Model ensemble simulations of CO_2 mixing ratios

Here, we present CO_2 mixing ratio simulations using the STILT model driven with different WRF experiments. The standard deviation among these simulations indicates the extent of uncertainty due to differences in the meteorological fields caused by

https://doi.org/10.5194/egusphere-2023-2334
Preprint. Discussion started: 6 March 2024

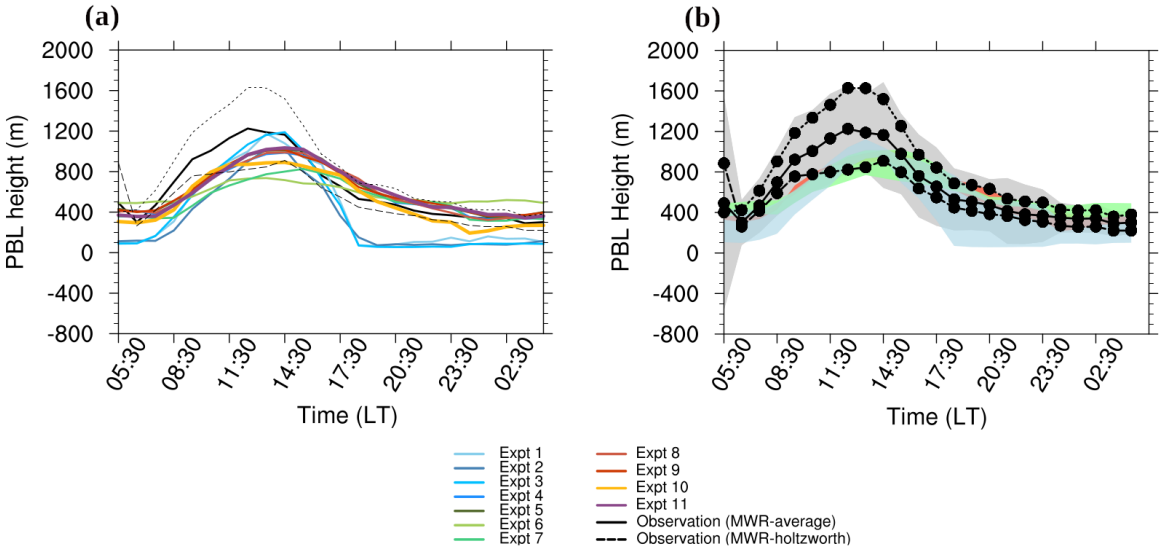

Figure 8. a) Monthly averaged diurnal variation of PBLH over Cochin for May 2017 for different experiments. b) Same as Fig. 2 but for PBLH, black line = MWR observation data with grey shade showing ± standard deviation from observation, shades of blue, green, and salmon shades show the range of values (maximum and minimum) obtained from Set 1, 2, and 3 experiments, respectively.

Table 3. PBLH comparison between observation and model simulations.

Expt.no	R^2				RMSE (m)				MBE (m)			
	t1	t2	t3	t4	t1	t2	t3	t4	t1	t2	t3	t4
Expt.1	0.91	0.87	0.77	0.02	237.35	296.07	305.69	245.03	-202.43	-195.03	-292.94	-232.39
Expt.2	0.86	0.93	0.21	0.1	353.3	302.16	330.85	269.49	-329.63	-275.01	330.85	-259.23
Expt.3	0.89	0.96	0.48	0.31	226.08	300.16	345.95	270.03	-174.22	-219.57	-338.95	-261.84
Expt.4	0.83	0.88	0.85	0.29	233.16	119.68	56.16	65.26	-212.14	99.86	56.16	5.15
Expt.5	0.81	0.92	0.91	0.38	211.27	123.18	60.92	68.54	-183.86	112.168	56.63	26.7
Expt.6	0.85	0.76	0.78	0.04	369.26	141.59	117.32	161.73	-334.45	-56.93	117.32	140.5
Expt.7	0.72	0.87	0.69	0.06	383.59	90.08	68.4	78.59	-362.09	18.76	45.98	-24.82
Expt.8	0.81	0.88	0.96	0.21	231.47	134.08	53.03	69.01	-207.11	116.07	53.03	8.31
Expt.9	0.86	0.89	0.88	0.49	203.78	104.81	78.49	69.87	-183.56	85.23	73.8	29.5
Expt.10	0.92	0.79	0.95	0.34	255.42	84.85	85.21	106.7	-245.96	21.98	85.21	-85.58
Expt.11	0.81	0.96	0.98	0.1	222.72	133.74	83.55	74.31	-194.46	126.01	79.36	1.68

https://doi.org/10.5194/egusphere-2023-2334
Preprint. Discussion started: 6 March 2024

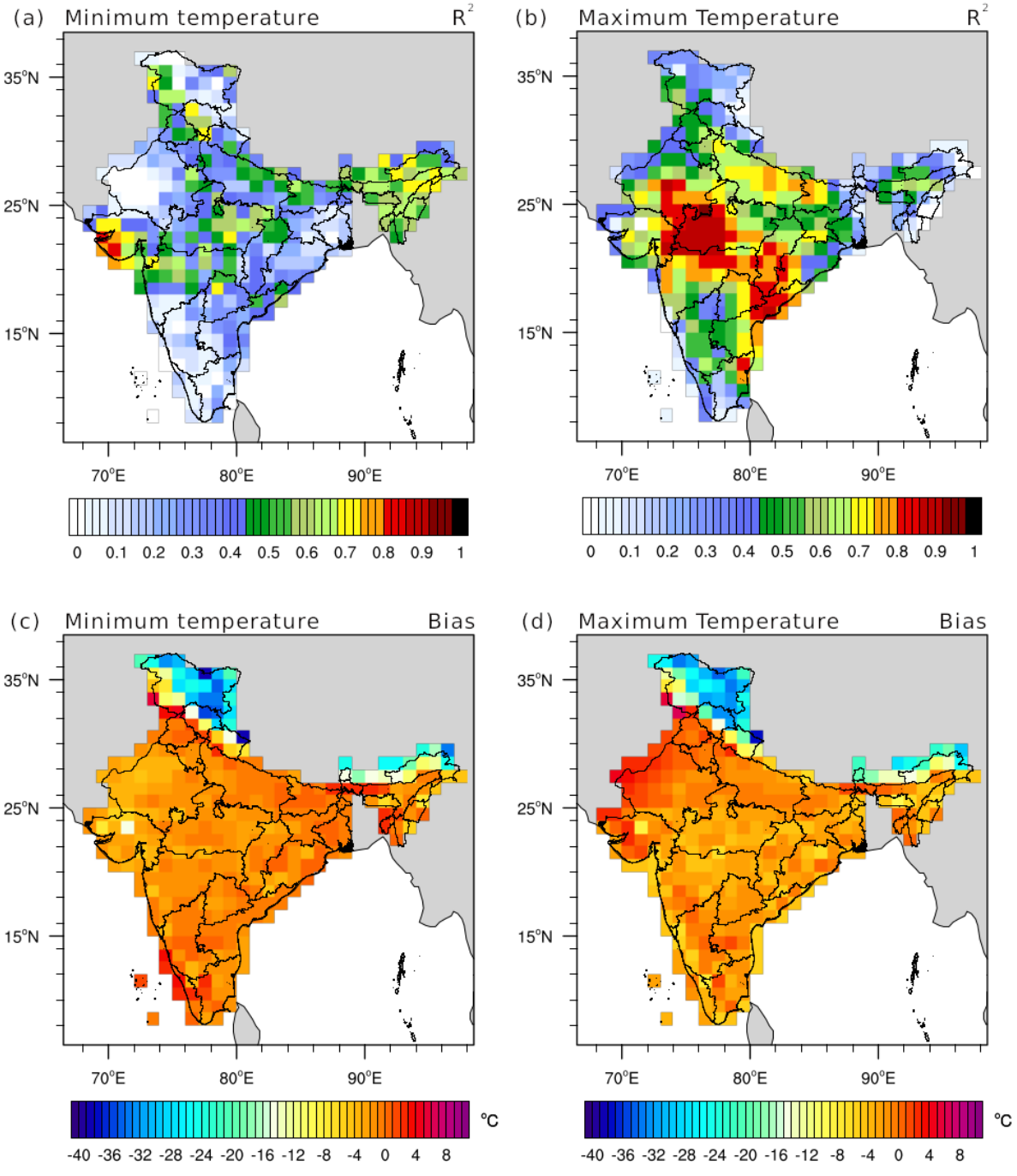

Figure 9. Spatial distribution of squared correlation coefficients and bias in monthly averaged simulations of maximum and minimum temperatures at 2 m in May 2017. a) & b) Maximum temperature: R^2 and bias, respectively and c) & d) Minimum temperature: R^2 and bias, respectively. Expt. 1 simulations and IMD dataset (data is only available for the Indian region) are used here.

https://doi.org/10.5194/egusphere-2023-2334
Preprint. Discussion started: 6 March 2024

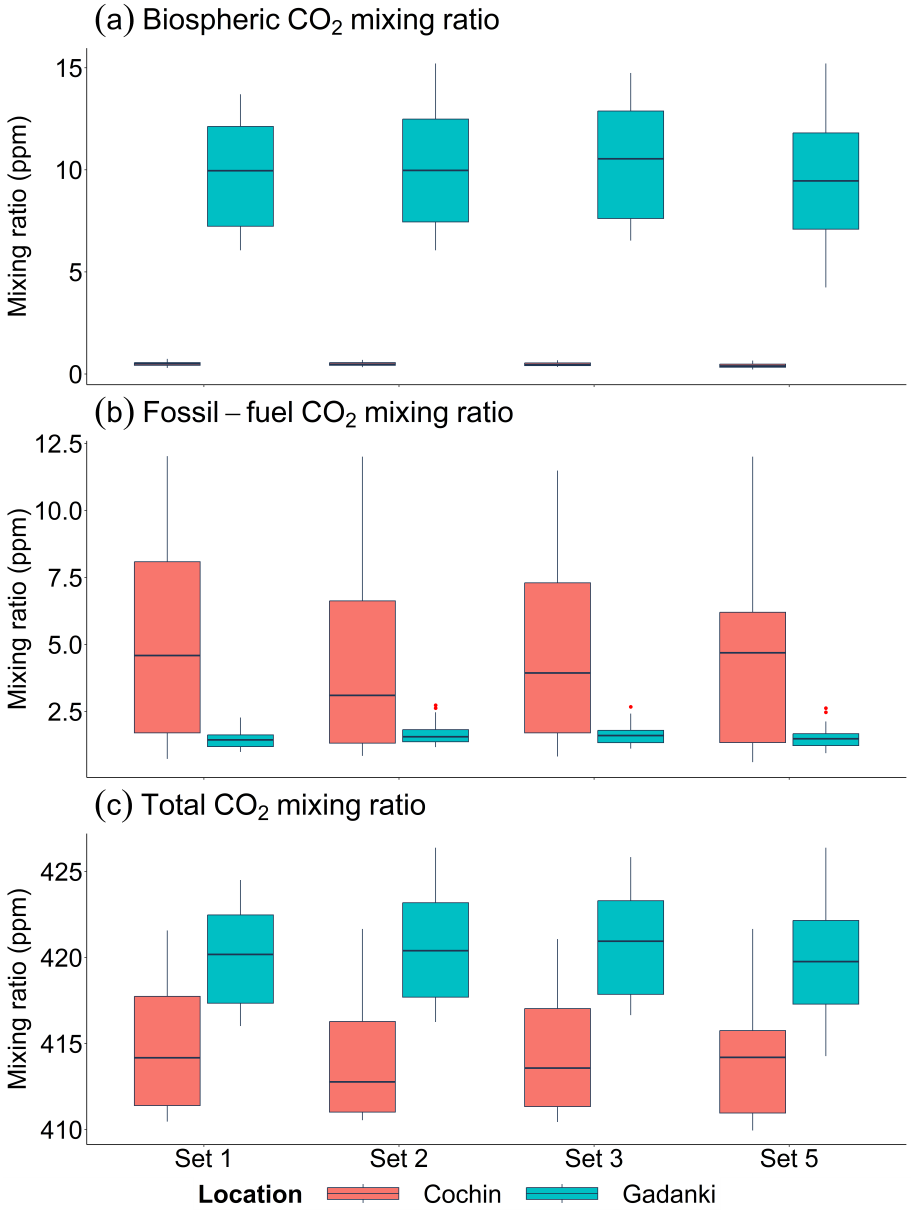

Figure 10. Variations in CO_2 mixing ratio simulations due to different meteorological model realizations over Cochin and Gadanki.

https://doi.org/10.5194/egusphere-2023-2334
Preprint. Discussion started: 6 March 2024

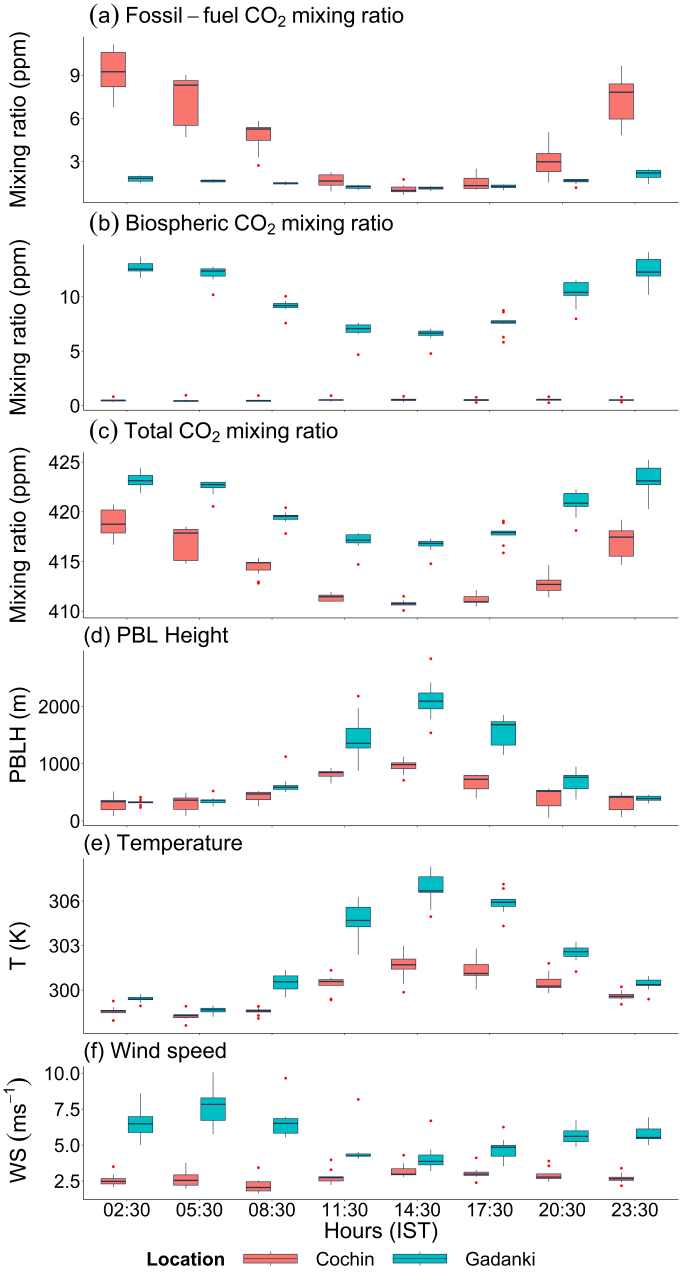

Figure 11. The model spread, calculated using 11 model ensemble members at each 3 hourly time step, for a) fossil-fuel CO_2, b) biospheric CO_2, c) total CO_2, d) PBL height, e) temperature and f) windspeed over Gadanki and Cochin.

https://doi.org/10.5194/egusphere-2023-2334
Preprint. Discussion started: 6 March 2024

various model realizations. The average uncertainty in total CO_2 mixing ratios owing to differences in simulating meteorological fields is 3.2 ppm (ranges from 0 to 24.3 ppm) for Cochin and 2.8 ppm (ranges from 0.2 to 10.8 ppm) for Gadanki. The larger variability in total CO_2 mixing ratios over Cochin compared to Gadanki indicates the influence of the coastal boundary layer on tracer transport. Fig 10 shows the variability caused by the different transport model parameterizations on the CO_2 mixing ratio simulations over Cochin and Gadanki. Over Cochin (urban), the spread (difference between interquartile ranges 75% and 25%) in total CO_2 is the largest in Set 1 (6.4 ppm), followed by Set 3 (5.8 ppm), Set 2 (5.3 ppm), and Set 5 (4.9 ppm). On the other hand, the spread is largest over Set 3 (5.6 ppm), followed by Set 2 (5.5 ppm), Set 1 (5.2 ppm), and Set 5 (5.0 ppm) for Gadanki (rural). As expected, Cochin is dominated by the contribution from $ffCO_2$. In the case of Gadanki, the biospheric contribution is significant. The diurnal distribution of model spread for these two sites is given in Fig. 11. For Cochin, total CO_2 shows the diurnal model spread of up to 4.5 ppm, with a strong contribution from fossil CO_2 (Fig. 11). In the case of Gadanki, the total CO_2 shows a diurnal model spread of up to 5 ppm, while the biospheric CO_2 shows a diurnal variability of 3.9 ppm. While the interquartile range of model spread in daytime total CO_2 has a variability of up to 0.6 ppm and 0.82 ppm, the nocturnal model spread ranges up to 2.5 and 1.6 ppm over Cochin and Gadanki.

As expected, the distribution of total CO_2 variability is well correlated with air temperature, PBL height, and windspeed for both sites (Fig. 11). Our results show that 58% of variability in $ffCO_2$ over Cochin and 69% of variability in bio-CO_2 over Gadanki are resulting from the variability in the PBL height simulations among different meteorological experiments.

4 Discussions

The present study gives an assessment of the impact of meteorological errors on CO_2 simulations by performing ensemble simulations of meteorological variables using the WRF model and CO_2 using the WRF-STILT model. The error diagnosis considered the relative contribution of model physics, PBL parameterization, model resolution, and initial meteorological state to the total error.

All model simulations capture the diurnal patterns in surface temperature and relative humidity irrespective of the scheme and parameterization used (R^2> 0.75 for both sites). Cochin, a coastal region, experiences drastic relative humidity variations compared with Gadanki, which is relatively dry in May. These small-scale variations in RH over the coastal city are not captured well by most models (Fig. S2). Among all models, Expt. 4 (using ACM2 PBL scheme) shows better performance for surface temperature and RH at both locations. Such betterment is also reported by (Gunwani and Mohan, 2017). While examining the impact of LSMs on simulations, all surface variables show considerable sensitivity to changes in LSMs (Set 2). Using the Unified Noah LSM (Set 1) resulted in better performance in terms of surface temperature and humidity (See Fig. 2). Interestingly, different models show the largest inter-model spread in surface temperature and RH during the afternoon hours, which decreases at night. The coupling of UCM to LSM seems to improve the model performance in simulating surface temperature and RH in the coastal urban region. Feng et al. (2016) and Nehrkorn et al. (2013) suggest the similar improvement in the overall performance of WRF.

https://doi.org/10.5194/egusphere-2023-2334
Preprint. Discussion started: 6 March 2024

In terms of wind predictions, the coupling of the UCM to LSM seems to be advantageous. Expt. 9 (with the UCM and the Noah-MP LSM) performed best in simulating the surface wind speed (See Fig. S2). In general, the models overestimate the wind speed at 10 m. While the models captured surface wind speed, most showed issues in reproducing diurnal variations in the wind direction, irrespective of the different advanced schemes used. The wind is highly influenced by local fluctuations resulting from land surface heterogeneity, and simulations of wind are largely affected by the poor representation of surface drag or roughness in the model. These issues are well documented in numerous studies (Karlický et al., 2018; Droste et al., 2018; Huang et al., 2019). Further, the associated changes in atmospheric dynamics can alter the mixing and dispersion of trace gases and pollutants (Huszar et al., 2020; Xiaolan Li and Zhao, 2019; Trusilova et al., 2016). As expected, the differences in PBL, LSM, and UCM significantly influenced the dynamics at the lower vertical levels (0 to 2 km) than at higher altitude levels. Due to the significant influence of shallow boundary layer structure, vertical wind profiles showed a larger influence of model schemes and parameterizations during evening hours than during morning times (See Fig. 3 & 6). The comparatively considerable impacts of model scheme differences on wind simulations are associated with orography. These orographically-driven fine-scale variations are difficult to reproduce by the model, irrespective of different combinations of model schemes. For example, wind patterns generated by large surface roughness can be offset by increased turbulence, convection and spurious mixing (Droste et al., 2018). The above scenario becomes challenging for the models to represent these simultaneous and counteracting effects adequately. Many model configurations, in general, are capable of only representing a subset of these effects.

Statistically significant improvements for the diurnal variations in surface temperature and relative humidity are noticed when the horizontal resolution of the model increases from 10 km to 3 km (See Figs. 2 & S2, Table 2, comparison between Expt. 6 and 10). More realistic simulations of vertical profiles of atmospheric variables can be expected when allowing the model to capture the subgrid variability (See Figs. 6a & 6b). Thilakan et al. (2022) discuss the importance of subgrid variability in the Indian region. Sensitivity towards changing horizontal resolution has been identified in the simulations of the verrtical profiles, as well.

The inter-model differences among ensemble simulations of CO_2 mixing ratios are considerable and indicate the extent to which the uncertainty in numerical weather prediction models influences the atmospheric transport of trace gases (Peylin et al., 2011). In our error estimations, we minimized the impact of other sources on the derived transport uncertainty of CO_2 by using the same set of local fluxes and the initial and lateral tracer fields. In the case of local contributions, temporal variations from the biospheric and anthropogenic fluxes also need to be considered, which may rectify the impact of transport uncertainty. In the case of total CO_2, there is an influence of the background mixing ratios (e.g., nonlocal fluxes) in addition to the local fluxes (biospheric and anthropogenic fluxes). Even if there are variations in the contribution of local fluxes to the mixing ratio (e.g., rectifier effect), their impact on the total CO_2 mixing ratio simulations is expected to be much less than that of meteorology. Peylin et al. (2011) reported a monthly average uncertainty of 0.8 ppm in the fossil CO_2 over Europe due to the transport error alone. Here we report the monthly averaged diurnal spread (interquartile range) of the fossil CO_2 1.5 ppm over Cochin. Between Cochin and Gadanki, the former has complex meteorology due to coastal influence (Hamza et al., 2007), resulting in large CO_2 uncertainty (up to 24 ppm). The large spread in CO_2 mixing ratio enhancement simulations (Fig. 11) during early

https://doi.org/10.5194/egusphere-2023-2334
Preprint. Discussion started: 6 March 2024

morning and late evening hours is attributed to the difficulty in simulating the atmospheric dynamics of the stable and shallow PBL. When comparing both stations, Gadanki shows less spread and more evident diurnal variability than Cochin, particularly during stable atmospheric hours (Fig. 11). Over Cochin, the spread in the trace gas mixing ratio (total CO_2) simulations is relatively large, which can also be attributed to the consistently lower wind speed over Cochin. Further, during the nighttime, when the wind speed is again lower than the daytime, the spread becomes large (Fig. 11). This indicates that the lower wind speed scenario increases the transport model uncertainty. Larger uncertainty in CO_2 enhancement simulations at nighttime (up to 4 ppm and 2.6 ppm over Cochin and Gadanki, respectively) compared to daytime (0.6 ppm and 1 ppm over Cochin and Gadanki, respectively) is attributed to the diurnal variability associated with the uncertainty in the simulated atmospheric PBLH. Our results for coastal urban and rural sites show that the trace gas enhancement simulations are significantly influenced by the modelled evolution of PBL and wind.

5 Conclusions

Understanding the distribution of the carbon sources and sinks requires accurate transport modelling of atmospheric CO_2. The capability of models to simulate meteorological fields is critical to the accuracy of atmospheric transport of trace gases. Here, we examined the potential of the WRF model to capture the observed meteorological variations that are crucial for tracer transport and thus relevant to inverse modelling of CO_2. We assessed the sensitivity of simulated meteorological fields to different schemes and parameterizations with a focus on designing appropriate WRF model setups over the region. Different model realizations enabled us to generate WRF simulations with eleven ensemble members and their comparison against observations, which were utilized further to assess CO_2 transport uncertainties originating from differences in meteorological realizations. The observational sites used, Cochin and Gadanki, represent urban and rural environments, respectively. Also, we extended our models' comparison to observational-based gridded data and reanalyzed products over the Indian subcontinent.

The analysis of the meteorological evaluation results, which involve both surface and vertical profile measurements, can be used to address the models' ability to simulate the CO_2 atmospheric transport in urban and rural environments. The diurnal variability patterns in the surface temperature and relative humidity are well captured at both urban and rural sites. The models capture the wind speed fairly well ($R^2 > 0.5$) with slightly overestimating wind speed. Vertical variations in RH and temperature are also reproduced by the simulations ($R^2 > 0.85$ for both variables), with higher model performance during the day than during the night. The vertical profiles of zonal and meridional winds are captured reasonably well by the model ensemble members, subjected to altitude levels. Cochin, being a coastal urban site, is highly influenced by terrain-induced transport features and urban meteorology, resulting in models to better represent Gadanki than Cochin. The general underestimation of the WRF wind speed towards the ground is likely due to improper representation of the surface roughness features and boundary layer dynamics in the model. Model performances are more sensitive to LSMs when compared to different PBL schemes. The vertical profiles show that the inter-model differences decrease with height, implying a relatively large influence of the LSMs in the surface simulations. The above inference is particularly relevant when we need a realistic representation of urban meteorology, given that more urban greenhouse gas measurement sites are planned.

https://doi.org/10.5194/egusphere-2023-2334
Preprint. Discussion started: 6 March 2024

As a consequence of differences in meteorological fields, atmospheric CO_2 uncertainty over Cochin is 3.2 ppm (statistically significant maximum: 24.3 ppm) and 2.8 ppm over Gadanki (statistically significant 10.8 ppm). Modelling issues with PBL cause large CO_2 modelling uncertainties of more than a factor of 3 to 5 during nighttime than daytime, and the urban site is significantly affected by the existence of low wind speed, creating more accumulation of trace gases causing high CO_2 modelling uncertainties. In this study, we provide an estimation of CO_2 uncertainties merely due to meteorological errors for the proper accounting of them in the carbon assimilation system. The analysis underscores the need to address atmospheric transport uncertainties in the carbon data assimilation framework over India to utilize the full potential of the observations. Given the potential of WRF to reproduce the meteorological variables relevant to CO_2 transport, we conclude that WRF can be used as a potential transport model for CO_2 inverse modelling studies. However, we advocate for a future study involving CO_2 observations and modelling (with different meteorology and flux realizations) for assessing the full strength and weakness of the models. The results from our study can be used while designing the inverse model using complex atmospheric mesoscale transport models like WRF for a desired application and characterising the transport error structures.

Code and data availability. The WRF version 3.9.1.1 source code developed by the WRF-ARW community is publicly available at https://doi.org/10.5065/D6MK6B4K. The STILT v2.3 model code can be accessed at https://projects.bgc-jena.mpg.de/STILT/svn/trunk with prior approval from the developers (last access: 10 April 2023, Lin et al. (2003)). The ERA5 surface level data are available at https://doi.org/10.24381/cds.adbb2d47 (Hersbach et al., 2018a, 2020) and variables at vertical pressure levels are given at https://doi.org/10.24381/cds.bd0915c6 (Hersbach et al., 2018b, 2020). The NCEP FNL data are available at https://doi.org/10.5065/D65Q4T4Z (last access: 10 April 2023). The EDGAR v7.0 data used in this study are publicly available at https://edgar.jrc.ec.europa.eu/dataset_ghg70 (last access: 10 April 2023; Crippa et al. (2021)). WRF and STILT simulations and the observational data from Cochin and Gadanki used for this study can be accessed at https://doi.org/10.5281/zenodo.10727298. IMD observation data can also be accessed here.

Author contributions. DP designed the study. TAM and AR performed the analysis and led the manuscript writing. LS performed the WRF model simulations and JSK performed the STILT model simulations. TAM, AR, DP, LS, and JSK interpreted the results. MMG provided a part of the observation data. MMG and VT contributed significantly to improve the manuscript. All authors discussed the results, reviewed the entire manuscript, and made relevant comments for improvement

Competing interests. All authors declare that they have no competing interest to disclose.

Acknowledgements. This study has been supported by the funding from the Max Planck Society allocated to the Max Planck Partner Group at IISERB, utilised as Junior Research Fellowship (JRF) to Lekshmi S. Also, Thara Anna Mathew acknowledges the financial support provided by the Scientific Education and Research Board (SERB) as JRF funding and further the University Grant Commision (UGC) and the Prime

https://doi.org/10.5194/egusphere-2023-2334
Preprint. Discussion started: 6 March 2024

Minister's Research Fellows (PMRF) Scheme for providing fellowship for PhD. We acknowledge IISERB institute funding supported by MHRD for PhD scholarship of Aparnna Ravi and Vishnu Thilakan and also the Council of Scientific and Industrial Research (CSIR) funding for Jithin. Also, we acknowledge the support of IISERB's high-performance cluster system, for computations, data analysis, and visualization. Special thanks to Dr. Thara Prabhakaran who leads the Cloud Aerosol Interaction and Precipitation Enhancement Experiment (CAIPEEX) project at IITM, Pune and Dr. K. Mohankumar, retired director of ACARR, Cochin for providing required observational data from joint-monsoon campaign of 2017. The authors thank Monish V. Deshpande for his contribution to the graphics.

https://doi.org/10.5194/egusphere-2023-2334
Preprint. Discussion started: 6 March 2024

References

Agustí-Panareda, A., Diamantakis, M., Massart, S., Chevallier, F., Muñoz-Sabater, J., Barré, J., Curcoll, R., Engelen, R., Langerock, B., Law, R. M., et al.: Modelling CO_2 weather–why horizontal resolution matters, Atmospheric Chemistry and Physics, 19, 7347–7376, 2019.

Ahmadov, R., Gerbig, C., Kretschmer, R., Körner, S., Rödenbeck, C., Bousquet, P., and Ramonet, M.: Comparing high resolution WRF-VPRM simulations and two global CO_2 transport models with coastal tower measurements of CO_2, Biogeosciences, 6, 807–817, 2009.

Benjamin, S. G., Grell, G. A., Brown, J. M., Smirnova, T. G., and Bleck, R.: Mesoscale weather prediction with the RUC hybrid isentropic–terrain-following coordinate model, Monthly Weather Review, 132, 473–494, 2004.

Bergamaschi, P., Karstens, U., Manning, A. J., Saunois, M., Tsuruta, A., Berchet, A., Vermeulen, A. T., Arnold, T., Janssens-Maenhout, G., Hammer, S., et al.: Inverse modelling of European CH_4 emissions during 2006–2012 using different inverse models and reassessed atmospheric observations, Atmospheric Chemistry and Physics, 18, 901–920, 2018.

Berrisford, P., Kållberg, P., Kobayashi, S., Dee, D., Uppala, S., Simmons, A., Poli, P., and Sato, H.: Atmospheric conservation properties in ERA-Interim, Quarterly Journal of the Royal Meteorological Society, 137, 1381–1399, 2011.

Bhati, S. and Mohan, M.: WRF-urban canopy model evaluation for the assessment of heat island and thermal comfort over an urban airshed in India under varying land use/land cover conditions, Geoscience Letters, 5, 1–19, 2018.

Boadh, R., Satyanarayana, A., Krishna, T. R., and Madala, S.: Sensitivity of PBL schemes of the WRF-ARW model in simulating the boundary layer flow parameters for their application to air pollution dispersion modeling over a tropical station, Atmósfera, 29, 61–81, 2016.

Bonacquisti, V., Casale, G., Palmieri, S., and Siani, A.: A canopy layer model and its application to Rome, Science of the Total Environment, 364, 1–13, 2006.

Chawla, I., Osuri, K. K., Mujumdar, P. P., and Niyogi, D.: Assessment of the Weather Research and Forecasting (WRF) model for simulation of extreme rainfall events in the upper Ganga Basin, Hydrology and Earth System Sciences, 22, 1095–1117, 2018.

Chen, F., Kusaka, H., Tewari, M., Bao, J., and Hirakuchi, H.: Utilizing the coupled WRF/LSM/Urban modeling system with detailed urban classification to simulate the urban heat island phenomena over the Greater Houston area, in: Fifth Symposium on the Urban Environment, vol. 25, pp. 9–11, American Meteorological Society Vancouver, BC, Canada, 2004.

Coniglio, M. C., Elmore, K. L., Kain, J. S., Weiss, S. J., Xue, M., and Weisman, M. L.: Evaluation of WRF model output for severe weather forecasting from the 2008 NOAA Hazardous Weather Testbed Spring Experiment, Weather and Forecasting, 25, 408–427, 2010.

Crippa, M., Solazzo, E., Huang, G., Guizzardi, D., Koffi, E., Muntean, M., Schieberle, C., Friedrich, R., and Janssens-Maenhout, G.: High resolution temporal profiles in the Emissions Database for Global Atmospheric Research, Scientific data, 7, 121, 2020.

Crippa, M., Guizzardi, D., Solazzo, E., Muntean, M., Schaaf, E., Monforti-Ferrario, F., Banja, M., Olivier, J., Grassi, G., Rossi, S., et al.: GHG emissions of all world countries, Publications Office of the European Union., 2021.

de Arruda Moreira, G., Guerrero-Rascado, J. L., Bravo-Aranda, J. A., Benavent-Oltra, J. A., Ortiz-Amezcua, P., Róman, R., Bedoya-Velásquez, A. E., Landulfo, E., and Alados-Arboledas, L.: Study of the planetary boundary layer by microwave radiometer, elastic lidar and Doppler lidar estimations in Southern Iberian Peninsula, Atmospheric Research, 213, 185–195, 2018.

Dee, D. P., Uppala, S. M., Simmons, A. J., Berrisford, P., Poli, P., Kobayashi, S., Andrae, U., Balmaseda, M., Balsamo, G., Bauer, d. P., et al.: The ERA-Interim reanalysis: Configuration and performance of the data assimilation system, Quarterly Journal of the royal meteorological society, 137, 553–597, 2011.

https://doi.org/10.5194/egusphere-2023-2334
Preprint. Discussion started: 6 March 2024

Droste, A. M., Steeneveld, G. J., and Holtslag, A. A. M.: Introducing the urban wind island effect, Environmental Research Letters, 13, 094 007, 2018.

Feng, S., Lauvaux, T., Newman, S., Rao, P., Ahmadov, R., Deng, A., Díaz-Isaac, L. I., Duren, R. M., Fischer, M. L., Gerbig, C., et al.: Los Angeles megacity: a high-resolution land–atmosphere modelling system for urban CO_2 emissions, Atmospheric Chemistry and Physics, 16, 9019–9045, 2016.

Friedlingstein, P., O'sullivan, M., Jones, M. W., Andrew, R. M., Hauck, J., Olsen, A., Peters, G. P., Peters, W., Pongratz, J., Sitch, S., et al.: Global carbon budget 2020, Earth System Science Data, 12, 3269–3340, 2020.

Gelaro, R., McCarty, W., Suárez, M. J., Todling, R., Molod, A., Takacs, L., Randles, C. A., Darmenov, A., Bosilovich, M. G., Reichle, R., et al.: The modern-era retrospective analysis for research and applications, version 2 (MERRA-2), Journal of climate, 30, 5419–5454, 2017.

Gerbig, C., Lin, J., Wofsy, S., Daube, B., Andrews, A., Stephens, B., Bakwin, P., and Grainger, C.: Toward constraining regional-scale fluxes of CO_2 with atmospheric observations over a continent: 2. Analysis of COBRA data using a receptor-oriented framework, Journal of Geophysical Research: Atmospheres, 108, 2003.

Grell, G. A. and Freitas, S. R.: A scale and aerosol aware stochastic convective parameterization for weather and air quality modeling, Atmospheric Chemistry and Physics, 14, 5233–5250, 2014.

Gunwani, P. and Mohan, M.: Sensitivity of WRF model estimates to various PBL parameterizations in different climatic zones over India, Atmospheric research, 194, 43–65, 2017.

Guo, J., Zhang, J., Yang, K., Liao, H., Zhang, S., Huang, K., Lv, Y., Shao, J., Yu, T., Tong, B., Li, J., Su, T., Yim, S. H. L., Stoffelen, A., Zhai, P., and Xu, X.: Investigation of near-global daytime boundary layer height using high-resolution radiosondes: first results and comparison with ERA5, MERRA-2, JRA-55, and NCEP-2 reanalyses, Atmospheric Chemistry and Physics, 21, 17 079–17 097, 2021.

Gurney, K. R., Law, R. M., Denning, A. S., Rayner, P. J., Baker, D., Bousquet, P., Bruhwiler, L., Chen, Y.-H., Ciais, P., Fan, S., et al.: TransCom 3 CO_2 inversion intercomparison: 1. Annual mean control results and sensitivity to transport and prior flux information, Tellus B: Chemical and Physical Meteorology, 55, 555–579, 2003.

Hamza, V., Babu, C., and Sabin, T.: Characteristic study of the boundary layer parameters over the Arabian Sea and the Bay of Bengal using the QuikSCAT dataset, Advances in Atmospheric Sciences, 24, 631–643, 2007.

Hariprasad, K., Srinivas, C. V., Singh, A. B., Rao, S. V. B., Baskaran, R., and Venkatraman, B.: Numerical simulation and intercomparison of boundary layer structure with different PBL schemes in WRF using experimental observations at a tropical site, Atmospheric Research, 145, 27–44, 2014.

Hedelius, J. K., Liu, J., Oda, T., Maksyutov, S., Roehl, C. M., Iraci, L. T., Podolske, J. R., Hillyard, P. W., Liang, J., Gurney, K. R., et al.: Southern California megacity CO_2, CH_4, and CO flux estimates using ground-and space-based remote sensing and a Lagrangian model, Atmospheric Chemistry and Physics, 18, 16 271–16 291, 2018.

Hersbach, H., Bell, B., Berrisford, P., Biavati, G., Horányi, A., Muñoz Sabater, J., Nicolas, J., Peubey, C., Radu, R., Rozum, I., et al.: ERA5 hourly data on single levels from 1979 to present, Copernicus climate change service (c3s) climate data store (cds), 10, 2018a.

Hersbach, H., de Rosnay, P., Bell, B., Schepers, D., Simmons, A., Soci, C., Abdalla, S., Alonso-Balmaseda, M., Balsamo, G., Bechtold, P., et al.: Operational global reanalysis: progress, future directions and synergies with NWP, 2018b.

Hersbach, H., Bell, B., Berrisford, P., Hirahara, S., Horányi, A., Muñoz-Sabater, J., Nicolas, J., Peubey, C., Radu, R., Schepers, D., et al.: The ERA5 global reanalysis, Quarterly Journal of the Royal Meteorological Society, 146, 1999–2049, 2020.

https://doi.org/10.5194/egusphere-2023-2334
Preprint. Discussion started: 6 March 2024

Holzworth, G. C.: Estimates of mean maximum mixing depths in the contiguous United States, Monthly Weather Review, 92, 235–242, 1964.

Hong, S.-Y., Dudhia, J., and Chen, S.-H.: A revised approach to ice microphysical processes for the bulk parameterization of clouds and precipitation, Monthly weather review, 132, 103–120, 2004.

Hu, X.-M., Nielsen-Gammon, J. W., and Zhang, F.: Evaluation of three planetary boundary layer schemes in the WRF model, Journal of Applied Meteorology and Climatology, 49, 1831–1844, 2010.

Huang, M., Gao, Z., Miao, S., and Chen, F.: Sensitivity of urban boundary layer simulation to urban canopy models and PBL schemes in Beijing, Meteorology and Atmospheric Physics, 131, 1235–1248, 2019.

Huszar, P., Karlický, J., Ďoubalová, J., Nováková, T., Šindelářová, K., Švábik, F., Belda, M., Halenka, T., and Žák, M.: The impact of urban land-surface on extreme air pollution over central Europe, Atmospheric Chemistry and Physics, 20, 11 655–11 681, 2020.

Inness, A., Ades, M., Agustí-Panareda, A., Barré, J., Benedictow, A., Blechschmidt, A.-M., Dominguez, J. J., Engelen, R., Eskes, H., Flemming, J., et al.: The CAMS reanalysis of atmospheric composition, Atmospheric Chemistry and Physics, 19, 3515–3556, 2019.

Janić, Z. I.: Nonsingular implementation of the Mellor-Yamada level 2.5 scheme in the NCEP Meso model, 2001.

Janjić, Z. I.: The step-mountain coordinate: Physical package, Monthly weather review, 118, 1429–1443, 1990.

Janjić, Z. I.: The step-mountain eta coordinate model: Further developments of the convection, viscous sublayer, and turbulence closure schemes, Monthly weather review, 122, 927–945, 1994.

Jiménez, P. A., Dudhia, J., González-Rouco, J. F., Navarro, J., Montávez, J. P., and García-Bustamante, E.: A revised scheme for the WRF surface layer formulation, Monthly weather review, 140, 898–918, 2012.

Jin, J. and Wen, L.: Evaluation of snowmelt simulation in the Weather Research and Forecasting model, Journal of Geophysical Research: Atmospheres, 117, 2012.

Kadaverugu, R., Matli, C., and Biniwale, R.: Suitability of WRF model for simulating meteorological variables in rural, semi-urban and urban environments of Central India, Meteorology and Atmospheric Physics, 133, 1379–1393, 2021.

Kalra, S., Kumar, S., and Routray, A.: Simulation of heavy rainfall event along east coast of India using WRF modeling system: impact of 3DVAR data assimilation, Modeling Earth Systems and Environment, 5, 245–256, 2019.

Kariyathan, T., Pillai, D., Elias, E., and Mathew, T. A.: On deriving influences of upwind agricultural and anthropogenic emissions on greenhouse gas concentrations and air quality over Delhi in India: A stochastic Lagrangian footprint approach, Journal of Earth System Science, 129, 1–15, 2020.

Karlický, J., Huszár, P., Halenka, T., Belda, M., Žák, M., Pišoft, P., and Mikšovský, J.: Multi-model comparison of urban heat island modelling approaches, Atmospheric Chemistry and Physics, 18, 10 655–10 674, 2018.

Keppel-Aleks, G., Wennberg, P., and Schneider, T.: Sources of variations in total column carbon dioxide, Atmospheric Chemistry and Physics, 11, 3581–3593, 2011.

Kottayil, A., Mohanakumar, K., Samson, T., Rebello, R., Manoj, M., Varadarajan, R., Santosh, K., Mohanan, P., and Vasudevan, K.: Validation of 205 MHz wind profiler radar located at Cochin, India, using radiosonde wind measurements, Radio Science, 51, 106–117, 2016.

Kusaka, H. and Kimura, F.: Coupling a single-layer urban canopy model with a simple atmospheric model: Impact on urban heat island simulation for an idealized case, Journal of the Meteorological Society of Japan. Ser. II, 82, 67–80, 2004.

Kusaka, H., Kondo, H., Kikegawa, Y., and Kimura, F.: A simple single-layer urban canopy model for atmospheric models: Comparison with multi-layer and slab models, Boundary-layer meteorology, 101, 329–358, 2001.

https://doi.org/10.5194/egusphere-2023-2334
Preprint. Discussion started: 6 March 2024

Lawrence, D. M., Oleson, K. W., Flanner, M. G., Thornton, P. E., Swenson, S. C., Lawrence, P. J., Zeng, X., Yang, Z.-L., Levis, S., Sakaguchi, K., et al.: Parameterization improvements and functional and structural advances in version 4 of the Community Land Model, Journal of Advances in Modeling Earth Systems, 3, 2011.

Lee, S.-H., Kim, S.-W., Angevine, W., Bianco, L., McKeen, S., Senff, C., Trainer, M., Tucker, S., and Zamora, R.: Evaluation of urban surface parameterizations in the WRF model using measurements during the Texas Air Quality Study 2006 field campaign, Atmospheric Chemistry and Physics, 11, 2127–2143, 2011.

Li, X. and Pu, Z.: Sensitivity of numerical simulation of early rapid intensification of Hurricane Emily (2005) to cloud microphysical and planetary boundary layer parameterizations, Monthly Weather Review, 136, 4819–4838, 2008.

Lian, J., Wu, L., Bréon, F.-M., Broquet, G., Vautard, R., Zaccheo, T. S., Dobler, J., and Ciais, P.: Evaluation of the WRF-UCM mesoscale model and ECMWF global operational forecasts over the Paris region in the prospect of tracer atmospheric transport modeling, Elementa: Science of the Anthropocene, 6, 2018.

Lin, J. and Gerbig, C.: Accounting for the effect of transport errors on tracer inversions, Geophysical Research Letters, 32, 2005.

Lin, J., Gerbig, C., Wofsy, S., Andrews, A., Daube, B., Davis, K., and Grainger, C.: A near-field tool for simulating the upstream influence of atmospheric observations: The Stochastic Time-Inverted Lagrangian Transport (STILT) model, Journal of Geophysical Research: Atmospheres, 108, 2003.

Lu, Y. and Kueppers, L. M.: Surface energy partitioning over four dominant vegetation types across the United States in a coupled regional climate model (Weather Research and Forecasting Model 3–Community Land Model 3.5), Journal of Geophysical Research: Atmospheres, 117, 2012.

Madala, S., Satyanarayana, A., and Tyagi, B.: Performance evaluation of convective parameterization schemes of WRF-ARW model in the simulation of pre-monsoon thunderstorm events over Kharagpur using STORM data sets, International Journal of Computer Applications, 71, 2013.

Madala, S., Satyanarayana, A., and Rao, T. N.: Performance evaluation of PBL and cumulus parameterization schemes of WRF ARW model in simulating severe thunderstorm events over Gadanki MST radar facility—case study, Atmospheric Research, 139, 1–17, 2014.

Madala, S., Satyanarayana, A., Srinivas, C., and Kumar, M.: Mesoscale atmospheric flow-field simulations for air quality modeling over complex terrain region of Ranchi in eastern India using WRF, Atmospheric Environment, 107, 315–328, 2015.

Manoj, M., Sivan, C., Rakesh, V., Rebello, R., Abhilash, S., and Mohankumar, K.: Atmospheric response to the annular solar eclipse of 26 December 2019 over Cochin, India, Advances in Space Research, 68, 3610–3621, 2021.

Mathew, T. A., Malap, N., Manoj, M., Jayarao, Y., Todekar, K., Rakesh, V., Rebello, R., Mohankumar, K., and Prabhakaran, T.: Pre-monsoon convective events and thermodynamic features of southwest monsoon onset over Kerala, India–A case study, Atmospheric Research, 248, 105 218, 2021.

Meyer, D., Schoetter, R., Riechert, M., Verrelle, A., Tewari, M., Dudhia, J., Masson, V., Van Reeuwijk, M., and Grimmond, S.: WRF-TEB: Implementation and evaluation of the coupled Weather Research and Forecasting (WRF) and Town Energy Balance (TEB) model, Journal of Advances in Modeling Earth Systems, 12.

Misenis, C., Hu, X., Krishnan, S., Zhang, Y., and Fast, J.: Sensitivity of WRF/Chem predictions to meteorological schemes, in: 86th Annual Conference/14th Joint Conference on the Applications of Air Pollution Meteorology with the A&WMA, Atlanta, GA, USA, vol. 27, 2006.

Mohan, M. and Bhati, S.: Analysis of WRF model performance over subtropical region of Delhi, India, Advances in Meteorology, 2011, 2011.

Mohan, M. and Sati, A. P.: WRF model performance analysis for a suite of simulation design, Atmospheric research, 169, 280–291, 2016.

https://doi.org/10.5194/egusphere-2023-2334
Preprint. Discussion started: 6 March 2024

Mohanakumar, K., Santosh, K., Mohanan, P., Vasudevan, K., Manoj, M., Samson, T. K., Kottayil, A., Rakesh, V., Rebello, R., and Abhilash, S.: A versatile 205 MHz stratosphere–troposphere radar at Cochin–scientific applications, Current Science, pp. 2459–2466, 2018.

Mukul Tewari, N., Tewari, M., Chen, F., Wang, W., Dudhia, J., LeMone, M., Mitchell, K., Ek, M., Gayno, G., Wegiel, J., et al.: Implementation and verification of the unified NOAH land surface model in the WRF model (Formerly Paper Number 17.5), in: Proceedings of the 20th conference on weather analysis and forecasting/16th conference on numerical weather prediction, Seattle, WA, USA, vol. 14, 2004.

Nakanishi, M. and Niino, H.: An improved Mellor–Yamada level-3 model with condensation physics: Its design and verification, Boundary-layer meteorology, 112, 1–31, 2004.

Nakanishi, M. and Niino, H.: An improved Mellor–Yamada level-3 model: Its numerical stability and application to a regional prediction of advection fog, Boundary-Layer Meteorology, 119, 397–407, 2006.

Nakanishi, M. and Niino, H.: Development of an improved turbulence closure model for the atmospheric boundary layer, Journal of the Meteorological Society of Japan. Ser. II, 87, 895–912, 2009.

Nath, D., Venkat Ratnam, M., Patra, A., Krishna Murthy, B., and Bhaskar Rao, S. V.: Turbulence characteristics over tropical station Gadanki (13.5 N, 79.2 E) estimated using high-resolution GPS radiosonde data, Journal of Geophysical Research: Atmospheres, 115, 2010.

Nehrkorn, T., Eluszkiewicz, J., Wofsy, S. C., Lin, J. C., Gerbig, C., Longo, M., and Freitas, S.: Coupled weather research and forecasting–stochastic time-inverted lagrangian transport (WRF–STILT) model, Meteorology and Atmospheric Physics, 107, 51–64, 2010.

Nehrkorn, T., Henderson, J., Leidner, M., Mountain, M., Eluszkiewicz, J., McKain, K., and Wofsy, S.: WRF simulations of the urban circulation in the Salt Lake City area for CO_2 modeling, Journal of Applied Meteorology and Climatology, 52, 323–340, 2013.

Niu, G.-Y., Yang, Z.-L., Mitchell, K. E., Chen, F., Ek, M. B., Barlage, M., Kumar, A., Manning, K., Niyogi, D., Rosero, E., et al.: The community Noah land surface model with multiparameterization options (Noah-MP): 1. Model description and evaluation with local-scale measurements, Journal of Geophysical Research: Atmospheres, 116, 2011.

Oleson, K. W., Lawrence, D. M., Bonan, G., Drewniak, B., Huang, M., Koven, C., Levis, S., Li, F., Riley, W. J., Subin, Z. M., et al.: Technical description of version 4.0 of the Community Land Model (CLM), NCAR Tech. Note NCAR/TN-478+ STR, 257, 2010.

Parazoo, N., Denning, A., Kawa, S., Corbin, K., Lokupitiya, R., and Baker, I.: Mechanisms for synoptic variations of atmospheric CO_2 in North America, South America and Europe, Atmospheric Chemistry and Physics, 8, 7239–7254, 2008.

Peylin, P., Houweling, S., Krol, M. C., Karstens, U., Rödenbeck, C., Geels, C., Vermeulen, A., Badawy, B., Aulagnier, C., Pregger, T., et al.: Importance of fossil fuel emission uncertainties over Europe for CO_2 modeling: model intercomparison, Atmospheric chemistry and physics, 11, 6607–6622, 2011.

Pillai, D., Buchwitz, M., Gerbig, C., Koch, T., Bovensmann, H., Reuter, M., and Burrows, J.: Inferring Source and Sink of Atmospheric CO_2 at High-resolution from Space: a Mesoscale Modeling Approach using Inverse Technique, in: EGU General Assembly Conference Abstracts, EGU General Assembly Conference Abstracts, pp. EGU2013–9818, 2013.

Pillai, D., Buchwitz, M., Gerbig, C., Koch, T., Reuter, M., Bovensmann, H., Marshall, J., and Burrows, J. P.: Tracking city CO_2 emissions from space using a high-resolution inverse modelling approach: a case study for Berlin, Germany, Atmospheric Chemistry and Physics, 16, 9591–9610, 2016.

Pleim, J. E.: A combined local and nonlocal closure model for the atmospheric boundary layer. Part I: Model description and testing, Journal of Applied Meteorology and Climatology, 46, 1383–1395, 2007.

Ragi, A., Sharan, M., and Haddad, Z.: Investigation of WRF's ability to simulate the monsoon-related seasonal variability in the thermodynamics and precipitation over southern peninsular India, Theoretical and Applied Climatology, 141, 1025–1043, 2020.

https://doi.org/10.5194/egusphere-2023-2334
Preprint. Discussion started: 6 March 2024

Raju, A., Parekh, A., Chowdary, J., and Gnanaseelan, C.: Assessment of the Indian summer monsoon in the WRF regional climate model, Climate Dynamics, 44, 3077–3100, 2015.

Reddy, G. K. K., Reddy, S. V., Sarojamma, B., and Ramkumar, T.: Statistical analysis for wind energy estimation over Gadanki, India, Research Journal of Engineering and Technology, 1, 30–40, 2015.

Rödenbeck, C., Zaehle, S., Keeling, R., and Heimann, M.: How does the terrestrial carbon exchange respond to inter-annual climatic variations? A quantification based on atmospheric CO_2 data, Biogeosciences, 15, 2481–2498, 2018.

Samson, T. K., Kottayil, A., Manoj, M., Binoy, B. B., Rakesh, V., Rebello, R., Vasudevan, K., Mohanan, P., Santosh, K., and Mohankumar, K.: Technical aspects of 205 MHz VHF mini wind profiler radar for tropospheric probing, IEEE Geoscience and Remote Sensing Letters, 13, 1027–1031, 2016.

Sathyanadh, A., Prabha, T. V., Balaji, B., Resmi, E., and Karipot, A.: Evaluation of WRF PBL parameterization schemes against direct observations during a dry event over the Ganges valley, Atmospheric Research, 193, 125–141, 2017.

Seidel, D. J., Zhang, Y., Beljaars, A., Golaz, J.-C., Jacobson, A. R., and Medeiros, B.: Climatology of the planetary boundary layer over the continental United States and Europe, Journal of Geophysical Research: Atmospheres, 117, 2012.

Sharma, A., Fernando, H. J., Hamlet, A. F., Hellmann, J. J., Barlage, M., and Chen, F.: Urban meteorological modeling using WRF: a sensitivity study, International Journal of Climatology, 37, 1885–1900, 2017.

Shepard, D.: Proceedings of the 1968 23rd ACM National conference, 1968.

Sivan, C., Rakesh, V., Abhilash, S., and Mohanakumar, K.: Evaluation of global reanalysis winds and high-resolution regional model outputs with the 205 MHz stratosphere–troposphere wind profiler radar observations, Quarterly Journal of the Royal Meteorological Society, 147, 2562–2579, 2021.

Skamarock, W. C. and Klemp, J. B.: A time-split nonhydrostatic atmospheric model for weather research and forecasting applications, Journal of computational physics, 227, 3465–3485, 2008.

Srivastava, A., Rajeevan, M., and Kshirsagar, S.: Development of a high resolution daily gridded temperature data set (1969–2005) for the Indian region, Atmospheric Science Letters, 10, 249–254, 2009.

Stull, R. B.: An introduction to boundary layer meteorology, vol. 13, Springer Science & Business Media, 1988.

Subin, Z., Riley, W., Jin, J., Christianson, D., Torn, M., and Kueppers, L.: Ecosystem feedbacks to climate change in California: Development, testing, and analysis using a coupled regional atmosphere and land surface model (WRF3–CLM3. 5), Earth Interactions, 15, 1–38, 2011.

Thilakan, V., Pillai, D., Gerbig, C., Galkowski, M., Ravi, A., and Anna Mathew, T.: Towards monitoring the CO_2 source–sink distribution over India via inverse modelling: quantifying the fine-scale spatiotemporal variability in the atmospheric CO_2 mole fraction, Atmospheric Chemistry and Physics, 22, 15 287–15 312, 2022.

Thilakan, V., Pillai, D., Sukumaran, J., Gerbig, C., Hakkim, H., Sinha, V., Terao, Y., Naja, M., and Deshpande, M. V.: Potential of using CO_2 observations over India in regional carbon budget estimation by improving the modelling system, EGUsphere, 2023, 1–32, 2023.

Torres, A. D., Keppel-Aleks, G., Doney, S. C., Fendrock, M., Luis, K., De Mazière, M., Hase, F., Petri, C., Pollard, D. F., Roehl, C. M., et al.: A geostatistical framework for quantifying the imprint of mesoscale atmospheric transport on satellite trace gas retrievals, Journal of Geophysical Research: Atmospheres, 124, 9773–9795, 2019.

Trusilova, K., Schubert, S., Wouters, H., Früh, B., Grossman-Clarke, S., Demuzere, M., and Becker, P.: The urban land use in the COSMO-CLM model: a comparison of three parameterizations for Berlin, Meteorologische Zeitschrift, 25, 231–244, 2016.

Uppala, S., Dee, D., Kobayashi, S., and Simmons, A.: Evolution of reanalysis at ECMWF, in: Proceedings of Third WCRP International Conference on Reanalysis, vol. 28, 2008.

https://doi.org/10.5194/egusphere-2023-2334
Preprint. Discussion started: 6 March 2024

Van der Molen, M. and Dolman, A.: Regional carbon fluxes and the effect of topography on the variability of atmospheric CO_2, Journal of Geophysical Research: Atmospheres, 112, 2007.

Vellalassery, A., Pillai, D., Marshall, J., Gerbig, C., Buchwitz, M., Schneising, O., and Ravi, A.: Using TROPOspheric Monitoring Instrument (TROPOMI) measurements and Weather Research and Forecasting (WRF) CO modelling to understand the contribution of meteorology and emissions to an extreme air pollution event in India, Atmospheric Chemistry and Physics, 21, 5393–5414, 2021.

Wang, L., Gong, W., Ma, Y., and Zhang, M.: Modeling regional vegetation NPP variations and their relationships with climatic parameters in Wuhan, China, Earth Interactions, 17, 1–20, 2013.

Wharton, S., Simpson, M., Osuna, J., Newman, J., and Biraud, S.: Assessment of Land Surface Model Performance in WRF for Simulating Wind at Heights Relevant to the Wind Energy Community, Tech. rep., Lawrence Livermore National Lab.(LLNL), Livermore, CA (United States), 2013.

Xiaolan Li, X.-M. H. Y. M. Y. W. L. L. and Zhao, Z.: Impact of planetary boundary layer structure on the formation and evolution of air-pollution episodes in Shenyang, Northeast China, Atmospheric Environment, 214, 116 850, 2019.

Yang, Z.-L., Niu, G.-Y., Mitchell, K. E., Chen, F., Ek, M. B., Barlage, M., Longuevergne, L., Manning, K., Niyogi, D., Tewari, M., et al.: The community Noah land surface model with multiparameterization options (Noah-MP): 2. Evaluation over global river basins, Journal of Geophysical Research: Atmospheres, 116, 2011.

Yver, C., Graven, H., Lucas, D. D., Cameron-Smith, P., Keeling, R., and Weiss, R.: Evaluating transport in the WRF model along the California coast, Atmospheric Chemistry and Physics, 13, 1837–1852, 2013.

Zhao, W. and Li, A.: A review on land surface processes modelling over complex terrain, Advances in Meteorology, 2015, 1–17, 2015.